THESIS

INVESTIGATION OF EXPOSURE RATE DISCREPANCIES BETWEEN ENERGY COMPENSATED GEIGER MUELLER TUBES AND PRESSURIZED IONIZATION CHAMBERS DUE TO MUON AND ANTI-MUON COSMIC PARTICLES

Submitted by

Matthew Gift

Department of Environmental and Radiological Health Sciences

In partial fulfillment of the requirements

For the Degree of Master of Science

Colorado State University

Fort Collins, Colorado

Summer 2017

Master's Committee:

Advisor: Thomas E. Johnson

Alexander Brandl
Gwenith Fisher

ABSTRACT

INVESTIGATION OF EXPOSURE RATE DISCREPANCIES BETWEEN ENERGY COMPENSATED GEIGER MUELLER TUBES AND PRESSURIZED IONIZATION CHAMBERS DUE TO MUON AND ANTI-MUON COSMIC PARTICLES

Energy compensated Geiger Mueller (GM) tubes and pressurized ionization chambers are two types of gas filled detectors that measure radiation dose or exposure but operate on different physical principles. Energy compensated GMs are gaining popularity because they are less expensive and more durable than pressurized ionization chambers, however, an exposure rate discrepancy may exist between the two instruments. At an elevation of about 1524m (5,000 ft), energy compensated GM tubes were observed to have nearly a 2-fold over-response to background measurements when compared to measurements performed by pressurized ionization chambers. The goal of this research is to investigate the expected exposure rate discrepancy due to muon and anti-muon cosmic particles, since they are the largest background contributor to dose at low elevations. Theoretically calculated average chord length and stopping power, as well as, Monte Carlo N-Particle 6 were used to investigate and characterize the exposure rate from muons and anti-muons. The calculated exposure rate contribution of muons and anti-muons for the background measurement of the energy compensated GM tube was negligible and is not expected to be the primary cause for the over-response. More research is needed to characterize the discrepancy.

ACKNOWLEDGEMENTS

I would like thank my committee members for patiently waiting for me to complete my research. A special thanks to my advisor Dr. Johnson for keeping me motivated and providing me with assistance throughout my research, your guidance has been invaluable to me. Also, Dr. Brandl for providing me with answers to the many physics and MCNP questions I had throughout the research. I cannot thank you enough, I would still probably be doing this research if it wasn't for you. In addition, thank you Dr. Rademacher for proposing the idea to investigate the exposure rate discrepancy between the two detectors for my thesis.

I would also like to thank a colleague of mine, Andrew Owens for providing me with MCNP help and helping me work through the many issues I ran into throughout the research. Also, John Wang for helping me obtain the ADM-300 from the Airforce Base in Cheyenne, Wyoming. Thank you to all of the representatives from Fluke Biomedical and Mirion Technologies for providing me with some information about the detectors. Last but certainly not least, I would like to thank the Mountain and Plains Education and Research Center and the Nuclear Regulatory Commission for funding me throughout this research.

TABLE OF CONTENTS

LIST OF TABLES

LIST OF FIGURES

Introduction

Motivation

Energy compensated Geiger Mueller (GM) tubes and pressurized ionization chambers (PIC) are two common instruments used to measure radiation dose and exposure. Both are gas filled detectors that operate using different physical principles. Energy compensated GM tubes are an event based instrument that utilizes fluence-to-dose conversions to obtain the radiation exposure. Pressurized ionization chambers on the other hand can measure radiation absorbed dose or exposure directly through ionization current that is formed from ionization in the gas due to incident radiation. Each instrument has its advantages and disadvantages.

Pressurized ionization chambers can measure radiation dose directly; however, they are very expensive and fragile, which can pose an issue if there is a restricted budget or one is performing rigorous field work. In addition, they can be sensitive to pressure changes which may be problematic if they are used in aircraft applications. (Rademacher, 2015)

Because of the negative qualities of the pressurized ionization chamber, energy compensated GM tubes are sometimes utilized for measuring dose or exposure. Energy compensated GM tubes are typically small, durable, low cost, and highly sensitive detectors that are ideal when performing work that requires robust, heavy duty instruments.

However, when a radiation dose or exposure is measured using both types of detectors, there can be a discrepancy between the measurements. The cause of the discrepancy is unknown but one hypothesis is that the discrepancy is due to muons. One of the primary concerns of the discrepancy is at low exposure rates, where the instrument is influenced to a reasonable extent from cosmic radiation sources, such as aircraft flight background exposure conditions. The underlying cause for the discrepancy must be characterized in order to understand the validity of dose or exposure assessments obtained using an energy compensated GM tube. The purpose of this project is to determine if the exposure rate discrepancy between the two types of instruments is in fact due to muons.

Radiation Physics Basics

Radioactivity may be defined as spontaneous nuclear transformation in unstable atoms that result in the formation of new elements (Cember, 2009). Each nuclear transformation is categorized by one of the following decay mechanisms: alpha emission, isobaric transitions, and isomeric transitions. The type of transition a radionuclide undergoes is determined mainly by nuclear instability and the available energy for the transition. Nuclear instability is a function of the ratio of neutrons to protons and the energy available is determined by the mass-energy relationship between the parent and daughter radionuclides and the emitted particles or waves. (Cember, 2009)

Decay Mechanisms

Alpha Emission

An alpha particle is a highly energetic Helium nucleus that is composed of two neutrons and two protons. Alpha emission occurs when it is energetically possible and an unstable atom has a neutron-to-proton ratio that is too low. During alpha emission, an alpha particle is emitted from an unstable nucleus resulting in the formation of a new element. The new element has an atomic mass number that is four less than the original radionuclide and an atomic number that is two less according to the following equation:

$$^{A}_{Z}P \rightarrow {}^{4}_{2}He + {}^{A-4}_{Z-2}D$$

The alpha particle emitted is essentially monoenergtic (Cember, 2009) but can be accompanied by gamma rays and consequently conversion electrons, Auger electrons, and/or characteristic X-rays if the nucleus is left in an excited state. Alpha emission typically occurs in elements with high atomic numbers (Z>82), and alpha particles are emitted with a minimum energy of 3.8 MeV based on energy considerations due to quantum tunneling through the potential barrier of the nucleus. There is one exception for the radionuclide Sa-142 which emits an alpha particle that has an energy of 2.18 MeV. (Brandl, 2015)

Isobaric Transitions

An isobaric transition occurs when the atomic mass number remains constant but the number of protons and neutrons varies between the parent radionuclide and its progeny. The type of isobaric transition determines how the number of protons and neutrons between the parent and daughter radionuclide will be impacted. The three types of isobaric transitions include beta emission, positron emission, and electron capture.

Beta emission is a type of isobaric transition that occurs in unstable atoms that have a neutron-to-proton ratio that is too high. During beta emission, a neutron is transformed into a proton which results in a highly energetic electron (beta particle) and an anti-neutrino emitted from the nucleus. Therefore, the progeny will have an atomic number that is increased by one but have an atomic mass number that remains unchanged to that of the parent radionuclide. Beta emission is represented by the equation below,

$$^{1}_{0}n \rightarrow {}^{1}_{1}p + {}^{0}_{-1}e + \bar{\nu}$$

Beta particles are emitted with a continuous energy distribution ranging from zero to a theoretical maximum based on the mass-energy relationship.

Positron emission is an isobaric transition that occurs in unstable atoms that have a neutron-to-proton ratio that is too low, and alpha emission is not energetically possible. Positron emission is the opposite of beta emission, in which a proton is transformed into a neutron which results in a positron and neutrino that are emitted from the nucleus. The progeny will have the same atomic mass number as the parent but will have a deficit of one proton. Thus, the atomic number of the daughter radionuclide will be one less than the parent radionuclide. Positron emission is represented by the equation below,

$$^{1}_{1}p \rightarrow {}^{1}_{0}n + {}^{0}_{1}e + \nu$$

The positrons disappear within a few microseconds depending on their energy and the electronic density of the medium. Within that time, the positron will interact with an electron, and the two particles will annihilate. The annihilation results in two gamma rays of equal but opposite magnitude that have energies equal to the mass-equivalent of the positron and electron pair. (Cember, 2009)

Electron capture is another type of isobaric transition that occurs in an atom that has a neutron-to-proton ratio that is too low. Electron capture competes with positron emission and alpha emission but has lower energy conservation requirements. Electron capture is the process where an inner atomic shell electron is captured by the nucleus, interacts with a proton and results in a neutron and neutrino. The result for the daughter nucleus is the same as positron emission in which the daughter radionuclide has an atomic number that is one less than the parent but the atomic mass number is constant. The following equation is a representation of electron capture:

$$ {}_{-1}^{0}e + {}_{1}^{1}p \rightarrow {}_{0}^{1}n + \nu $$

It should be noted that an Auger electron or a characteristic X-ray of the daughter radionuclide is also emitted as the vacant electron hole is filled with a higher energy electron.

Isomeric Transitions

Isomeric transitions are a type of radioactive decay that result in a loss of energy but have no effect on atomic number and atomic mass. The two types of isomeric transitions are gamma ray emission and internal conversion. Gamma ray emission occurs when an exited nucleus de-excites through the release of electromagnetic radiation in the form of a gamma ray. Gamma rays have no charge and consequently are not influenced by the coulombic force.

Internal conversion occurs when energy from an excited nucleus is transferred to a tightly bound electron causing the electron to be expelled from the atom. (Turner, 2007) Characteristic X-rays accompany internal conversion as higher energy shell electrons fill the vacancies in the tightly bound atomic shells of the radionuclide.

Radiation interactions with matter

As radiation traverses through matter it loses energy by means of excitation and ionization. The degree of energy loss is dependent on the type and energy of the radiation, as well as the characteristics of the traversed medium. (Cember, 2009) The factors above inherently determine the mechanism of energy loss and penetration power of the radiation. The particles and waves that are emitted from the decay mechanisms outlined above interact with matter by different means due to their size and charge characteristics.

Alpha Particles

Alpha particles are the least penetrating type of radiation due to their high charge and mass. They have a very high probability of interaction with matter through collisions and coulombic interactions. They primarily lose energy through interactions with orbital electrons, although energy can also be lost from nuclear collisions. (Brandl,2015) Alpha particles only transfer a small amount of energy per collision because of the conservation of energy and momentum but have a very high specific ionization due to their high probability of interaction. Therefore, they create a large number of ion pairs in the traversing medium, and deposit a lot of energy within a short length. Alpha particles essentially travel in a straight path losing energy continuously with little deviation from scattering. Alpha particles can generally be stopped by the dead layer of skin or a thin sheet of paper and pose no threat due to external radiation hazards.

Geiger Muller tubes only need a single ion pair formed within the fill gas to trigger a full Geiger discharge; therefore, their counting efficiency is essentially 100 percent for any charged particle that enters the active volume. (Knoll, 2012) Using a GM tube to detect alpha particles requires the instrument to have a very small window thickness, allowing the alpha particle to penetrate into the active volume and trigger a Geiger discharge. GM tubes only detect alpha particle interactions and are not intended to measure a dose or exposure rate due to alpha particles. A GM should not be used as an accurate assessment of dose or exposure rates from alpha particles.

Pressurized ionization chambers collect all the charges created by direct ionization within the gas by the electric field formed by the potential difference between the anode and cathode. Therefore, if an alpha particle has sufficient energy to penetrate the detector and chamber walls, it may create ionization within the gas. If ionization occurs, charge will be collected and a signal will be produced relating the ionization current to an exposure or dose rate.

Beta Particles

Beta particles mainly interact with matter through excitation and ionization. Similar to alpha particles, beta particles are charged and can interact through direct collisions and coulombic interactions. In contrast, betas have very large scattering angles from collisions and can lose all of their kinetic energy in a single collision based on the conservation of energy and momentum. The distance a beta particle can travel through a material is called its range and is mainly a function of the incident beta particle energy and areal density of the absorbing material. The range of a beta particle is also impacted by the atomic number of the absorbing medium.

Beta particles also interact with matter by producing bremsstrahlung radiation. Bremsstrahlung radiation is classified as a type of x-ray but is produced in a different manner than a characteristic x-ray. Bremsstrahlung radiation is produced when a beta particle passes near a nucleus and undergoes an acceleration as a result of a coulombic electrostatic interaction between the nucleus and the beta particle. The bremsstrahlung radiation is emitted tangentially with respect to the acceleration change and has a continuous energy spectrum ranging from the energy of the beta particle down to zero. (Brey, 2009)

Stopping power is the average linear rate of energy loss of a particle due to excitation and ionization in a medium. The stopping power of a particle traversing through a medium can be used to determine the dose delivered to the medium and can be related to the biological effectiveness of the type of radiation. (Turner, 2007) Beta particles have two contributions to stopping power, namely, radiative stopping power and collisional stopping power. The radiative stopping power contribution is from bremsstrahlung radiation and only becomes important at high energies. (Turner, 2007) The collisional stopping power contribution is from collisions between the particles and atomic electrons and nuclei. The rate of energy loss increases with decreased particle velocity and increased charge. (Cember, 2009)

Geiger Muller tubes are often available with a beta window allowing the instrument to detect beta particles that penetrate into the active volume. Similar to alpha particles, only a single ion pair formed within the fill gas can trigger a Geiger discharge, resulting in the efficiency of detecting beta particles at nearly 100 percent, if the window is open. Backscatter of beta particles traversing through the window can be an issue if the window thickness is a significant fraction of the electron range. (Knoll, 2012) GM tubes should only be utilized to detect beta radiation and should not be used as an accurate assessment of dose or exposure rates.

Similar to alpha particles, if a beta particle has enough energy to penetrate through the detector and chamber walls and produce ionization in the fill gas of the ionization chamber, charge will be collected and a signal relating to dose or exposure will be formed.

Photons

Photon interaction with matter is fundamentally different from beta and alpha particles. Both beta and alphas particles can be completely stopped in matter, whereas, photons can only be attenuated. Photons interact poorly with matter and can consequently penetrate great distances. The attenuation of photons in a medium is a function of the atomic number of the absorber, density of the absorbing material, and the kinetic energy of the photon. The three main mechanisms of photon interactions with matter are the photoelectric effect, Compton scattering, and pair production. The probability of each mechanism is based upon photon energy and the atomic number of the absorbing material.

The photoelectric effect occurs when a photon interacts with a tightly bound electron, transferring all of its energy to the electron, causing the photon to disappear. When the energy transferred to the electron is greater than its binding energy, the electron (photoelectron) is ejected from the atom and behaves similar to a beta particle, loosing energy through excitation and ionization of matter. Characteristic x-rays or Auger electrons accompany the photoelectric effect due to higher shell electrons filling vacancies created by the ejected electron. (Brey, 2009) The photoelectric effect favors low energy photons and high atomic number absorbers. (Cember, 2012)

Compton scattering occurs when a photon has an elastic collision with a “loosely” bound electron. The photon transfers some but not all of its energy to the electron which results in a scattered photon and a scattered electron (Compton electron). The energies of the scattered photon and Compton electron depend on the angle of scatter. The Compton electron loses energy in the same manner as a beta particle. (Cember, 2012) Compton scattering is more probable for low to medium energy incident photons and high atomic numbered absorbers.

Pair production occurs when a photon with energy greater than or equal to 1.022 MeV passes near the vicinity of a nucleus and spontaneously disappears, creating a positron and electron pair. Pair production can also take place in the vicinity of an electron but it is much less probable and requires a threshold energy of 2.044 MeV for the incident photon. Pair production favors high energy photons and high atomic numbered absorbers. (Cember, 2009) (Brey, 2009)

Photons are detected in a different manner in a GM tube since they are not charged particles and have a low probability of interaction. Most of the GMs response to photons arises from the interactions described above in the solid wall of the detector. When the wall interactions take place close to the active volume, secondary electrons created may reach the gas and create ions, resulting in a Geiger discharge. The probability that an incident photon interacts with the wall to produce a secondary electron and the probability the electron reaches the fill gas are the two separate factors that account for the efficiency of detecting photons in a GM tube. Photon counting efficiencies are rarely higher than several percent. (Knoll, 2012) Photons can also interact with the fill gas directly causing excitation and ionization but this is much more probable at low photon energies and high atomic number and fill gas pressure. GM tubes can function as a count rate instrument for detecting photons but may be calibrated in terms of exposure rate units, with error as high as a factor of 2 or 3 or more. (Knoll, 2012)

Pressurized ionization chambers primarily utilize photon wall interactions to measure a radiation dose or exposure. If the interaction occurs close to the wall of the detector, secondary electrons resulting from the interactions in the wall can produce ionization within the active volume of the chamber. The charges in the ionized gas will be collected by the anode and cathode producing an ionization current or signal, which is then converted to an exposure or dose rate. Direct ionization due to photons can also occur within the fill gas but is less probable.

Cosmic Radiation

Cosmic radiation is primarily radiation that is generated from outside the solar system but within the galaxy. The primary cosmic particles consist of about 90 percent protons, 9 percent alpha particles, and about 1 percent of heavier nuclei that are distinguished by their high energies. (Gaisser, 1990) Most cosmic radiation is relativistic in nature and can have energies up to 10^{20} eV. (Heinrich, 1999) As these highly energetic particles traverse through the atmosphere, they interact with atmospheric molecules producing secondary ionizing particles and waves. These secondary particles can have a wide spectrum of energies and are often in the form of protons, neutrons, and mesons. The mesons are usually short lived and decay into several other highly energetic elementary particles or photons. The primary and secondary particles continue to have successive interactions creating a cascade of hadrons and their decay products in the atmosphere. (Heinrich, 1999)

Cosmic rays fluence and energy are a function of altitude, geomagnetic location, and solar activity. Energy and fluence of cosmic rays generally increases with increasing altitude due to earth's atmosphere acting as a shield. At higher altitudes earth's atmosphere has a lower density thickness resulting in fewer interactions and attenuation and consequently higher energies than at low altitudes. Cosmic radiation is dependent upon geomagnetic location due to the deflection of the charged particles by earth's magnetic field. Cosmic radiation on earth is the highest at the poles due to the lack of shielding and re-direction of charged particles provided from the magnetic field. Cosmic radiation is inversely proportional to solar activity. Solar activity causes matter to be ejected from the sun resulting in high intensity solar wind. (Heinrich, 1999) The solar wind interacts with the cosmic radiation causing it to be attenuated.

Muons are a decay product of mesons. They have a mean lifetime of 2.2 microseconds and decay into an electron, a neutrino, and an electron anti-neutrino. (Serway, 2005) In a classical sense, they cannot reach the surface of the earth. However, due to relativistic principles, they penetrate deeply into the earth's surface. They have a small cross section for interaction, making them very penetrating. (Gaisser, 1990) At low altitudes, the muon component is the most important contributor to dose from cosmic radiation. (ICRU, 2010)

The hypothesis of the experiment is that muons and anti-muons are the cause of the exposure rate discrepancy between pressurized ionization chambers and energy compensated GM tubes. Monte Carlo N Particle 6 (MCNP6) from Los Alamos National Laboratory is the radiation transport code that will be used to investigate the exposure rate discrepancy between the two detectors. (Goorley, 2012) Once the discrepancy is characterized and understood, adjustments can then be made to the energy compensated GM detector to measure exposure rates equivalent to those measured from a pressurized ionization chamber. Thereby, allowing the use of a more affordable and durable detector in lieu of a pressurized ionization chamber.

Materials & Methods

451P Pressurized Ionization Chamber

MCNP 6 was used to simulate radiation transport of several different radiological sources, and results were compared to experimental data collected in room 119 of the Molecular and Radiological Bioscience (MRB) building at Colorado State University (CSU). The first detector that was used was a 451P-RYR pressurized micro-Roentgen ionization chamber survey meter manufactured by Fluke Biomedical. The serial number of the detector is 4337. A copy of the calibration spreadsheet can be found in Appendix A.

The sources used to collect the experimental data were gamma standard Type D disk sources from Eckert & Ziegler Analytics and are listed in Table 1.

Table 1: Sources used to collect experimental data.

Source	SRS Number	Activity [Bq]	Activity (μCi)
Am-241	92765	36260	0.98
Ba-133	92769	192400	5.2
Co-60	92768	188700	5.1
Cs-137	92766	188700	5.1
Mn-54	92770	188700	5.1

The activities presented in the table are reported as initial activities from February 20, 2013 at 12:00 PM eastern standard time. All sources had an active diameter of 0.5 cm (0.197 in) and a height of 0.32 cm (0.125 in) and were encapsulated in a high strength plastic that was 2.54 cm (1 in) in diameter and 0.635 cm (0.25 in) thick. The plastic window of each source was 0.28 cm (0.109 in) thick. (Point Sources, 2016) Each source was placed on the surface of the white dot located on the side of the detector and measurements were recorded in units of Roentgen per hour once the detector had a stabilized reading. A background measurement was also collected and used to obtain a net measured value. The net measured value was then used to validate the MCNP model.

MCNP 6 was used to build a simplified model of the detector. The model consisted of the plastic outer detector case, the plastic chamber wall, the plastic Type D disk source, and the active chamber volume of the detector. Estimates for the detector case thickness and diameter, height, and thickness of the chamber wall were provided by a representative at Fluke Biomedical. The density of the chamber wall used in the model was calculated from the 200 mg cm^{-2} density thickness provided in the 451P operator's manual. The detector case and chamber wall were assumed to be polyethylene and have a uniform thickness, and modeled as such. The input deck of the MCNP model was viewed in the Visual Editor software, VisEd. A cross-sectional top view of the model obtained from VisEd is shown in Figure 1.

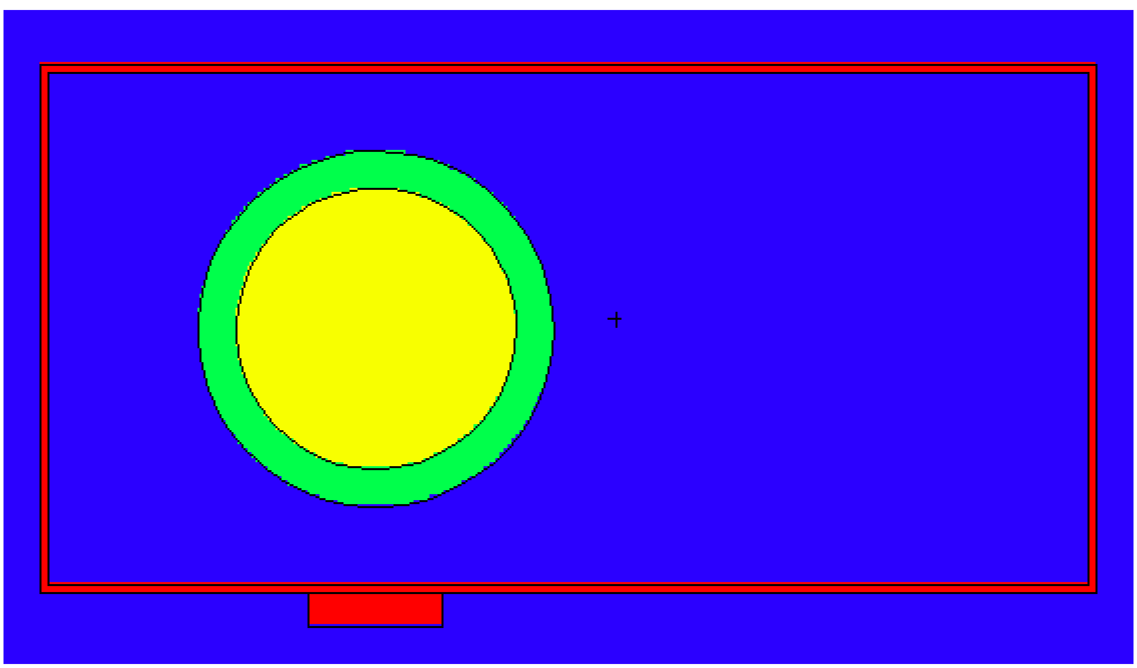

Figure 1: Cross-sectional top view of the simplified 451P pressurized ionization chamber.

Each material type used for the simulation, excluding the fill gas was obtained from *Compendium of Material Composition Data for Radiation Transport Modeling*. (McConn Jr.,2011) The material of the fill gas inside the chamber was created using the average composition of the nitrogen and argon mixture. The ideal gas law was then used to determine the density of the fill gas and to adjust it to account for the chamber pressurized to 8 ATM. The percent composition of the fill gas was assumed to be in terms of percent mass. The air density used for the model was interpolated at 1524 m (5,000 ft) which is about the elevation at which the experimental measurements were performed. (U.S Standard Atmosphere, 2017)

The 451P is designed to operate and respond to photons above 25 keV and beta radiation above 1 MeV. (Fluke Biomedical, 2013) Therefore, alpha particles were not simulated and only photons greater than 25 keV and beta particles and cascade electrons greater than 1 MeV were simulated in the model. Photons for Am-241 with an intensity below 1×10^{-4} percent were also not simulated since they contribute very little to the energy absorbed within the active volume of the detector. Photons and cascade electrons within the limits of the detector were obtained from the National Nuclear Data Center (NNDC) at Brookhaven National Laboratory (BNL) and were simulated in the model. (NNDC, 2015) Beta spectra for Cs-137 and Co-60 used in the simulation were obtained from *Availability of Nuclear Decay Data in Electronic Form.* (Eckerman, Westfall, Ryman, & Cristy, 1994) The simulated particle emission type, energy, and intensity is provided in Appendix B for each source simulated.

The MCNP input code was operated in P E mode for photons, beta particles, and cascade electrons. The P E mode enables the software to track the coupled transportation of photons and electrons. Ten million photons were simulated for each emission energy per source and a *F8 tally was used to determine the energy deposition in units of MeV per starting particle within the active volume. Beta distributions simulated for Cs-137 and Co-60 were performed with one hundred million particles and the same *F8 tally was used. The MCNP results for each energy were multiplied by their respective intensities and were superimposed to obtain the total energy deposition. The total energy deposition was then converted into Roentgen per hour by the following equation:

$$\dot{X} = \frac{(MCNP_{Result})\mathrm{MeV} \cdot (Activity_{Source})\mathrm{Bq} \cdot 1.602{\times}10^{-13}\,\frac{\mathrm{J}}{\mathrm{MeV}} \cdot 418{,}542\ \frac{\mathrm{R\ hr^{-1}}}{\mathrm{Gy\ s^{-1}}}}{228.249\ \mathrm{cm^3} \cdot 0.0102\,\frac{\mathrm{g}}{\mathrm{cm^3}} \cdot \frac{1\mathrm{kg}}{1000\mathrm{g}}}$$

Where, 228.249 cm^3 is the active volume of the chamber and 0.0102 g cm^{-3} is the pressure corrected density of the fill gas mixture. The unit conversion from Roentgen to Gray was based on Equation IA3 in ICRU Report 10b. (ICRU, 1962) The activity for each source was decay corrected to the time the experimental measurements were performed. The experimental data were then compared to the MCNP data. The MCNP values were then corrected with respect to the energy response curve by extrapolating values on a per energy basis and using them as a multiplicative factor to adjust the MCNP results. Once the model was validated, muon MCNP simulations and calculations were performed to determine the average energy deposition within the active volume of the chamber. A sample of an input code that was used to simulate betas is provided in Appendix C.

The muon and anti-muon sources were modeled as a sphere with a radius of ten meters centered at the active volume of the chamber. Both sources were directed inward and normal with respect to the sphere. The anti-muon and muon mean momenta and intensities were determined from *Measurements of Ground-Level Muons at Two Geomagnetic Location* (Kremer, 1999) and are shown below in Table 2.

Table 2: Anti-muon and muon mean momenta and intensities using CAPRICE 97 data. (Kremer, 1999)

Elevation: 1270m (4166.67 ft)					
Momentum Interval [MeV/c]	**Mean Momentum [MeV/c]**	**Anti-Muon [(GeV/c m^2 sr s)$^{-1}$]**	**Normalized Anit-Muon Intensity**	**Muon [(GeV/c m^2 sr s)$^{-1}$]**	**Normalized Muon Intensity**
200-300	250	12	6.841E-02	10.7	6.724E-02
300-400	350	17	9.691E-02	15.2	9.552E-02
400-550	470	20.3	1.157E-01	17.9	1.125E-01
550-700	620	21.2	1.209E-01	18.6	1.169E-01
700-850	780	20.4	1.163E-01	17.6	1.106E-01
850-1000	920	19.2	1.095E-01	16.4	1.031E-01
1000-1200	1100	17.7	1.009E-01	14.8	9.300E-02
1200-1400	1300	15.5	8.836E-02	12.8	8.044E-02
1400-1600	1500	13.9	7.924E-02	11.4	7.164E-02
1600-2100	1840	0	0.000E+00	9.2	5.781E-02
2100-2940	2490	7	3.991E-02	5.7	3.582E-02
2940-4120	3490	4.8	2.736E-02	3.86	2.426E-02
4120-5500	4780	2.94	1.676E-02	2.31	1.452E-02
5500-7000	6210	1.78	1.015E-02	1.37	8.609E-03
7000-10000	8370	1.02	5.815E-03	0.78	4.902E-03
10000-15500	12420	0.414	2.360E-03	0.32	2.011E-03
15500-23000	18850	0.154	8.779E-04	0.116	7.289E-04
23000-31100	26680	0.064	3.648E-04	0.045	2.828E-04
31100-43600	36690	0.028	1.596E-04	0.0203	1.276E-04
43600-61100	51470	0.0102	5.815E-05	0.0077	4.839E-05
61100-85600	72080	0.0042	2.394E-05	0.0032	2.011E-05
85600-120000	100960	0.0015	8.551E-06	0.0011	6.912E-06

The mean momentum and normalized intensities were used in the MCNP input file. The anti-muon and muon simulations had to be executed separately since MCNP can only support one starting particle type. The anti-muon simulation was performed in ! P mode and the muon simulation was performed in | P mode, and both simulations were run with one billion starting particles. A *F8 tally was used in both simulations to determine the energy deposition in units of MeV per starting particle. The resulting energy depositions from anti-muons and muons were summed to determine the total average energy deposition per starting particle, and the sum was compared to the energy deposition that was theoretically calculated from the product of collisional stopping power and chord length. An example of the muon input file is shown in Appendix D. The theoretical collisional stopping power was calculated according to the following equation (Turner, 2007):

$$-\frac{dE}{dx} = \frac{4\pi k_0^2 z^2 e^4 n}{mc^2\beta^2} \cdot \left[\ln\left(\frac{2mc^2\beta^2}{I(1-\beta^2)}\right) - \beta^2\right]$$

where

k_0 = 8.99 × 10^9 N m^2 C^{-20}
z = atomic number of the heavy particle (z = 1 for muons)
e = magnitude of the electron charge, 1.6 × 10^{-19} C
n = number of electrons per unit volume in the medium, $\sum_i N_i Z_i$
m = electron rest mass, 9.109 × 10^{-31} kg
c = speed of light in vacuum, 2.998 *x* 10^8 m/s
β = v/c = speed of the particle relative to c
I = mean excitation energy of the medium,

Values for β^2 were derived using the total energy equation for relativistic particles, $E = \gamma mc^2 = E_k + mc^2$. (Serway, 2005) The rest mass energy, $E = mc^2$, for muons and anti-muons was calculated at 105.7 MeV. The mean excitation energy of the medium was calculated by $n\ln(I) = \sum_i N_i Z_i \ln(I_i)$, where N_i is the number of atoms per cubic centimeter and Z_i is the atomic number of the i^{th} element. The mean excitation energies per element were calculated by the following empirical formulas (Turner, 2007):

$$I_i \cong \begin{cases} 19.0\ \text{eV}, & Z = 1 \\ 11.2 + 11.7(Z)\text{eV}, & 2 \leq Z \leq 13 \\ 52.8 + 8.71(Z)\text{eV}, & Z > 13 \end{cases}$$

The radiative stopping power was not taken into consideration since radiative effects do not become a large contribution to the total stopping power of muons until about 1000 GeV/c. (Amsler, 2010)

The average chord length, $\overline{L}$ of the active volume of the detector was calculated by the following equation (Borak, 1994):

$$\overline{L} = \frac{4V}{S}$$

Where *V* is the active volume of the detector, and *S* is the surface area of the active volume.

The resulting exposure rate due to muons and anti-muons in the ionization chamber was then calculated by the following equation:

$$\dot{X} = \frac{(FLuence\ Rate)_{Total}\,\frac{\text{Particles}}{\text{cm}^2\text{s}} \cdot A\ \text{cm}^2 \cdot (Energy\ Deposition)\ \text{keV} \cdot 1.602 \times 10^{-16}\ \frac{\text{J}}{\text{keV}} \cdot 86\,\frac{\text{R}}{\text{Gy}} \cdot 3600\,\frac{\text{s}}{\text{hr}}}{228.249\ \text{cm}^3 \cdot 0.0102\,\frac{\text{g}}{\text{cm}^3} \cdot \frac{1}{1000}\,\frac{\text{kg}}{\text{g}}}$$

The total fluence rate is the combination of the fluence rates of muons and anti-muons and *A* is the cross-sectional area of the active volume.

ADM-300

The energy compensated GM tube that was used to collect experimental data was an ADM-300 multi-functional survey meter manufactured by Canberra Industries of Mirion Technologies. The ADM-300 can be used as a stand-alone instrument or can be coupled with external probes depending on the application. The ADM-300 was operated as the stand-alone instrument to utilize the two internal energy compensated GM tubes to measure exposure rates. The ADM-300 used was obtained from Francis E. Warren Air Force Base located in Cheyenne, Wyoming and the serial number for the detector is ADM-690331. The detector was calibrated by Bionetics Corporation using a Cs-137 source and responded within ±15 percent of the true value up to 250 Roentgen per hour. The certificate of calibration is provided in Appendix E.

The sources used to collect the experimental data were the same as the data collected with the pressurized ionization chamber and are shown in Table 1. Each source was placed 2.54 cm (1 in) away from the "x" located on the side of the detector and measurements were recorded once a stabilized reading was observed. A background measurement was also taken in order to calculate a net measurement that was used to validate the MCNP model. All readings were taken with the beta window closed.

MCNP 6 was used to build a simplified model of the detector. Several assumptions were made to build the model. The active volumes of the energy compensated GM high energy and low energy tubes were placed in the center of the "x" on the side of the detector and the centered on the "H" and "L" on the bottom of the detector respectively. The percent composition of the fill gas was also estimated based upon the typical concentrations of quench gases, with values between 5 – 10 percent. (Knoll, 2012). A value of 92.5 percent was used for the primary fill gas and 7.5 percent for the quench gas. The model consisted of the outer detector case, the high and low range GM tubes, and their associated shielding for energy compensation, and the plastic Type D disk source. Figure 2 is a cross-sectional top view of the simplified model viewed in VisEd.

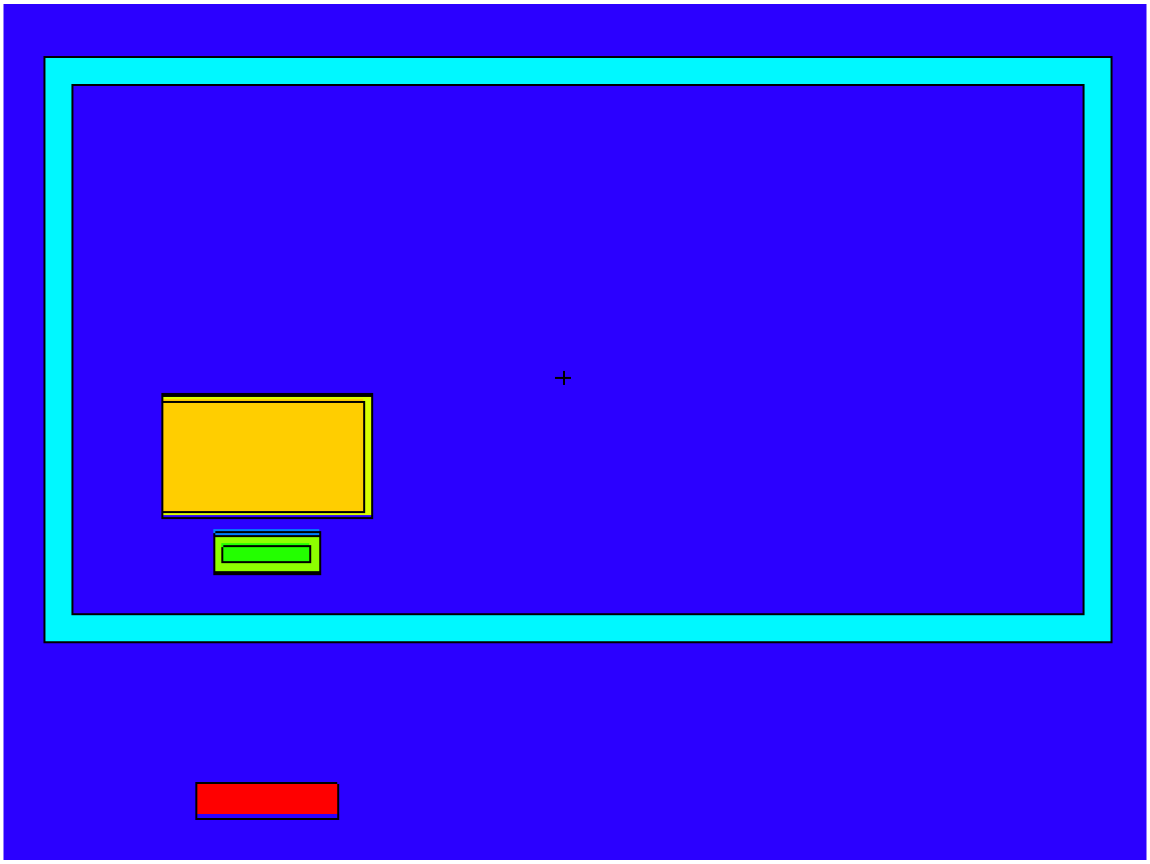

Figure 2: Cross-sectional top view of the simplified ADM-300 model.

The materials used to build the model, excluding the mica window and the fill gas were found from *Compendium of Material Composition Data for Radiation Transport Modeling*. (McConn Jr.,2011) The material for the fill gas for each GM tube was created based on the estimated average composition of the primary fill gas and quench gas. The ideal gas law was used to determine the density of the gas and also to pressure correct the tubes to the proper specifications. The material card for mica was created based on the mole ratio of muscovite mica compound, $KAl_3Si_3O_{10}(OH)_2$. (Minerals, 2017) The air density used for the model was interpolated at 5,000 feet using the same data as the 451P model.

The energy response limits of operation for the ADM-300 were not listed in the operator's manual or Canberra's website and were also not provide upon request. Energy specifications for the ADM-300 were found online from Southern Scientific website. (ADM, 2017) Southern Scientific reports an energy response from 80 keV to 3 MeV for gamma radiation. Therefore, photons above 80 keV were simulated for each particle. The operator's manual for the ADM specifies "ADM-300 is intended for beta radiation detection only. The dose rate indicated is not accurate for beta radiation." Therefore, beta radiation and cascade electrons were not simulated. Alpha radiation was also not simulated because it cannot penetrate into the active volumes of the detector. No simulation was performed for Am-241 because no exposure rate was registered on the detector. The photons simulated within the limits of the detector were obtained from the NNDC and are shown in Appendix F, with their respective energies and intensities. (NNDC,2015)

The MCNP input code was simulated in P E mode to validate the MCNP model and to obtain a fluence rate to exposure rate conversion. Ten million photons were simulated using F4 tallies to determine the fluence through the high range and low range GM tubes respectively, for each energy per source. All tallies had respective tally multiplier cards that consisted of the intensity for each energy multiplied by the decay corrected activity for each source. The output of the tallies was in units of particles per centimeter squared per second. The results from the tallies from each tube were added for each energy, and the resulting values for the high and low range tube were summed to obtain a total fluence rate through the active volumes of the detector. The conversion from fluence rate to exposure rate could not be provided by Canberra, so it was estimated from the measured value of Cs-137 divided by the total MCNP Cs-137 fluence result. Cs-137 was chosen because the detector was calibrated to a Cs-137 source. All total fluence rate results from each source were then multiplied by the estimated fluence rate to exposure rate conversion to obtain an exposure rate in units of R h^{-1}. The exposure rates calculated from the high and low range GM tubes were then corrected by values extrapolated from the energy response curves of the tubes for a more accurate comparison between the model and the measurement.

Once the model was "validated", muon and anti-muon MCNP simulations and calculations were performed to determine the average energy deposition within the active volume of the GM tubes. The anti-muon and muon mean momenta and intensities used in the simulation were the same as those used for 451P and are shown in Table 2. The same modes and tallies were used as the pressurized ionization chamber simulations. Due to high uncertainty, five billion particles were run for each anti-muon and muon simulation. The resulting energy deposition from the simulation was compared to the product of collisional stopping power and average chord length, using the same method as the pressurized ionization chamber. Again, the radiative stopping power contribution was not taken into consideration. Sample input models for the ADM-300 were omitted due to the non-disclosure agreement signed with Canberra Industries of Mirion Technologies.

The calculated energy deposition was then used to determine that enough energy was deposited in the active volumes to cause the GM tubes to fire. The next step was to calculate if a significant or negligible contribution of the background measurement was due to muons and anti-muons. The average background measurement was divided by the estimated fluence rate to exposure rate conversion, in order to obtain a fluence rate in units of particles per square centimeter per second through both of the GM tubes. The fluence rate was multiplied by the combined cross-sectional areas of both tubes to determine the number of particles per second that pass through the active volumes, assuming that all particles that pass through cause the GM to fire. The cross-sectional areas were combined because there was no way to distinguish which particles passed through either the high range or the low range tube to create the signal in the detector. The resulting number was then compared to the number of muons and anti-muons that pass through the active detector volumes. The number of muons and anti-muons that pass through the GM tubes was determined from the fluence rates from *Measurements of Ground-Level Muons at Two Geomagnetic Locations*. (Kremer, 1999) The fluence rates from Kremer were given in units of particles per GeV/c m^2 sr s. Each fluence rate for both muons and anti-muons was multiplied by their respective energies, and the square meters were converted into square centimeters. Then all values were multiplied by 2 pi, assuming that the detector is a fixed target and scattering is constrained to the forward direction of the detector. It also assumes that the distribution of final state particles is isotropic.[1] The resulting values were then multiplied by the combined cross-sectional areas of the active volumes of the high and low energy tubes. The values were summed to obtain the total number of anti-muons and muons that pass through the total active volume of the ADM-300.

[1] Personal communication, Dr. N. Buchanan, Colorado State University Physics Department, June, 2017

Results

Figure 3 depicts the discrepancy between pressurized ionization chambers and energy compensated GM tubes.

Figure 3: Background measurements showing a discrepancy between the dose rate measured with a Ludlum Model 9DP pressurized ionization chamber and exposure rate from the ADM-300.

Although, the Ludlum Model 9DP pressurized ionization chamber was not modeled in the study, Figure 3 is shown for illustrative purposes. Methodology from ICRU Report 10b was used to convert the background dose rate in units of µSv h^{-1} to an exposure rate. The calculated exposure rate measured with the Ludlum Model 9DP was 15.1 µR h^{-1}. Therefore, the discrepancy in exposure rates between the two detectors was approximately 10 µR h^{-1}. Measurement discrepancies for the sources outlined in Table 1 between the two detectors shown in Figure 3 are provided in Appendix H.

451P Pressurized Ionization Chamber

Table 3 contains the measured exposure rates obtained with the Fluke Biomedical 451P pressurized ionization chamber using the sources from Table 1.

Table 3: Exposure rates in roentgen per hour measured with the 451P pressurized ionization chamber.

Source	Measurement [R/hr]	Average Background [R/hr]	Net Measurement [R/hr]
Am-241	2.70E-05	1.20E-05	1.50E-05
Ba-133	2.90E-04	1.20E-05	2.78E-04
Co-60	1.07E-03	1.20E-05	1.06E-03
Cs-137	4.20E-04	1.20E-05	4.08E-04
Mn-54	4.30E-05	1.20E-05	3.10E-05

The average background exposure rate was subtracted from the measured exposure rates to result in net measured values that were used to validate the MCNP model.

The MCNP results for each energy per source are provided in Appendix I. All results obtained from the photon, beta, and cascade electrons MCNP simulations have an associated uncertainty of less than 3 percent. Table 4 below the comparison of the net measured value versus the values calculated from the MCNP model.

Table 4: Comparison of the net measured value versus the MCNP model from the 451P pressurized ionization chamber.

Radionuclide	Net Measured Value [R/hr]	MCNP Value [R/hr]	Measurement/MCNP	Percent Difference
Am-241	1.50E-05	9.12E-06	1.64	64.49
Ba-133	2.78E-04	5.33E-04	0.52	-47.83
Co-60	1.06E-03	1.13E-03	0.94	-6.37
Cs-137	4.08E-04	4.42E-04	0.92	-7.67
Mn-54	3.10E-05	3.28E-05	0.94	-5.59

The MCNP values were then corrected based on extrapolated values from the energy response curve for the 451P in order to have a more realistic comparison of the measured values from the detector and the energy deposition results obtained from the simulations. The energy response curve for the 451P is shown in Figure 4.

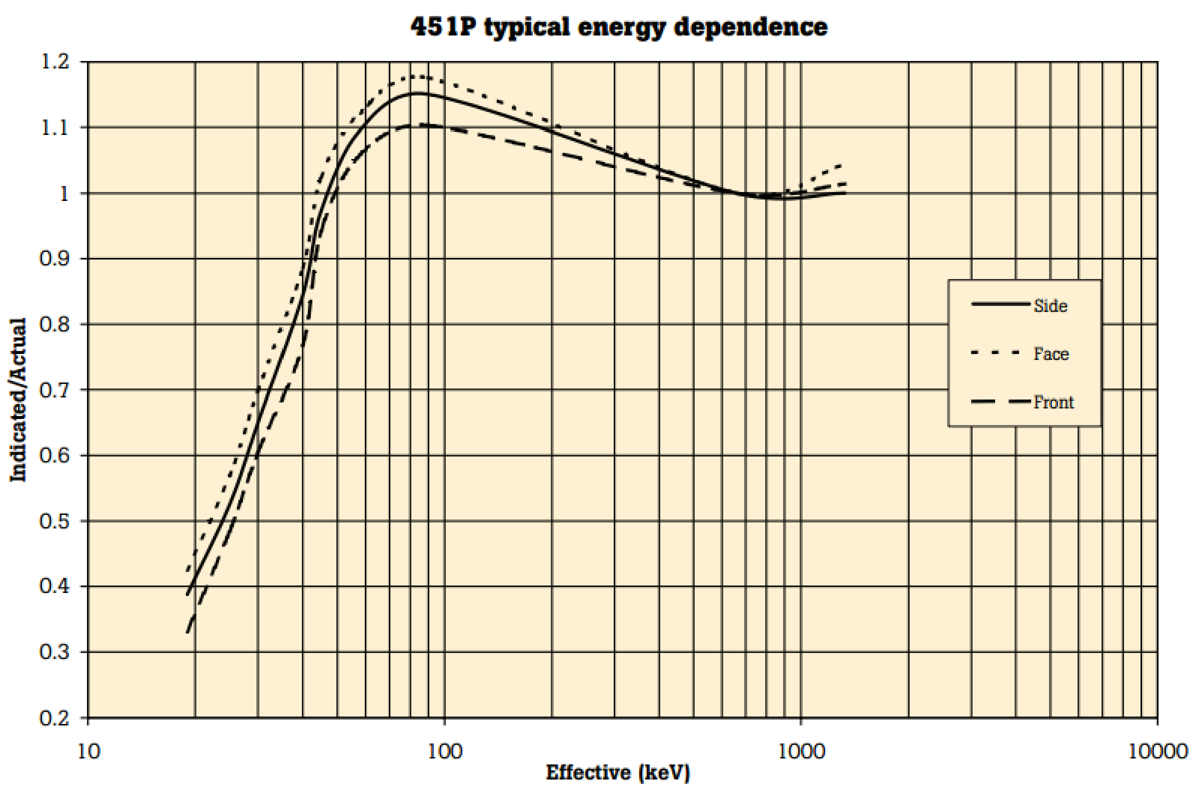

Figure 4: Energy response curve for the 451P pressurized ionization chamber. (Reproduced with permission from Fluke Biomedical. See Appendix M)

The values for the corrected MCNP result, as well as, the corresponding ratios and percent differences are shown in Table 5.

Table 5: Comparison of net measured values versus MCNP energy response corrected values for the 451P pressurized ionization chamber.

Radionuclide	Net Measured Value [R/hr]	Corrected MCNP Value [R/hr]	Measurement/MCNP	Percent Difference
Am-241	1.50E-05	9.04E-06	1.66	65.94
Ba-133	2.78E-04	4.50E-04	0.62	-38.27
Co-60	1.06E-03	1.13E-03	0.94	-6.37
Cs-137	4.08E-04	4.36E-04	0.94	-6.41
Mn-54	3.10E-05	3.25E-05	0.95	-4.64

Once the model was validated, a weighted collisional stopping power calculation was performed. The calculated results for the weighted collisional stopping powers are shown in Appendix I. The weighted average stopping powers for each energy were summed for the muons and anti-muons. The resulting values were then normalized and added to obtain a total weighted average collisional stopping power of about 2.17×10^{-2} MeV cm^{-1}. The average chord length for the active volume of the chamber was calculated at about 4.22 cm (1.66 in). The theoretical average energy deposition from cosmic muons and anti-muons within the active volume of the chamber was determined to be 9.16×10^{-2} MeV or about 92 keV. The resulting exposure rate due to the energy deposition for the muons and anti-muons in the 451P was 10.7 μR h^{-1} using the horizontal cross-sectional area with respect to the orientation of the detector. The exposure rate calculated using the vertical cross-sectional area of a plane with respect to the orientation of the chamber was 26.4 μR h^{-1}.

The theoretical average energy deposition was then compared to the energy deposition from the muon and anti-muon MCNP simulations. The energy deposition resulting from the *F8 tally for the muon simulation was 1.71×10^{-6} MeV with a 8.2 percent uncertainty and the result for the anti-muon simulation was 1.69×10^{-6} MeV with a 7.9 percent uncertainty. Therefore, the total average energy deposition per starting particle within the active volume of the chamber due to muons and anti-muons was 3.41×10^{-6} MeV from the simulation. The resulting exposure rates obtained from the MCNP results due to muons and anti-muons were 0.337 nR h^{-1} calculated from the horizontal cross-sectional area and 0.835 nR h^{-1} calculated from the vertical cross-sectional area.

ADM-300

Shown in Table 6 are the exposure rates measured from the ADM-300 operated using the energy compensated GM tubes. The sources used are outlined in Table 1.

Table 6: Exposure rates in roentgen per hour measured with the ADM-300.

Source	Measurement [R/hr]	Average Background [R/hr]	Net Measurement [R/hr]
Am-241	N/A	N/A	N/A
Ba-133	1.81E-04	3.30E-05	1.48E-04
Co-60	1.31E-03	3.30E-05	1.28E-03
Cs-137	3.78E-04	3.30E-05	3.45E-04
Mn-54	6.20E-05	3.30E-05	2.90E-05

The average background measurement was subtracted from the measured value to obtain a net measured value and was used to validate the MCNP model.

The MCNP results from each energy per source are provided in Appendix J. All simulations had an uncertainty of less than one percent for each energy. The fluence rate to exposure rate estimated from the Cs-137 measurement value and the F4 tally value from MCNP was calculated at 4.02×10^{-7} R h^{-1} per particle cm^{-2} s^{-1}. Table 7 provides a summary and comparison of the measured results and the simulated results.

Table 7: Comparison of the net measured values versus the MCNP model results from the ADM-300.

Radionuclide	Net Measured Value [R/hr]	MCNP Value [R/hr]	Measurement/MCNP	Percent Difference
Am-241	N/A	N/A	N/A	N/A
Ba-133	1.48E-04	3.18E-04	0.46	-53.63
Co-60	1.28E-03	5.27E-04	2.42	142.31
Cs-137	3.45E-04	3.45E-04	1.00	0.00
Mn-54	2.90E-05	1.61E-05	1.80	80.35

The MCNP values after the conversion from the fluence rate to exposure rate for the high and low range tubes were adjusted in reference to the energy response curves provided by Mirion ®[2]. Figure 5 shows the energy response curve for the low range tube.

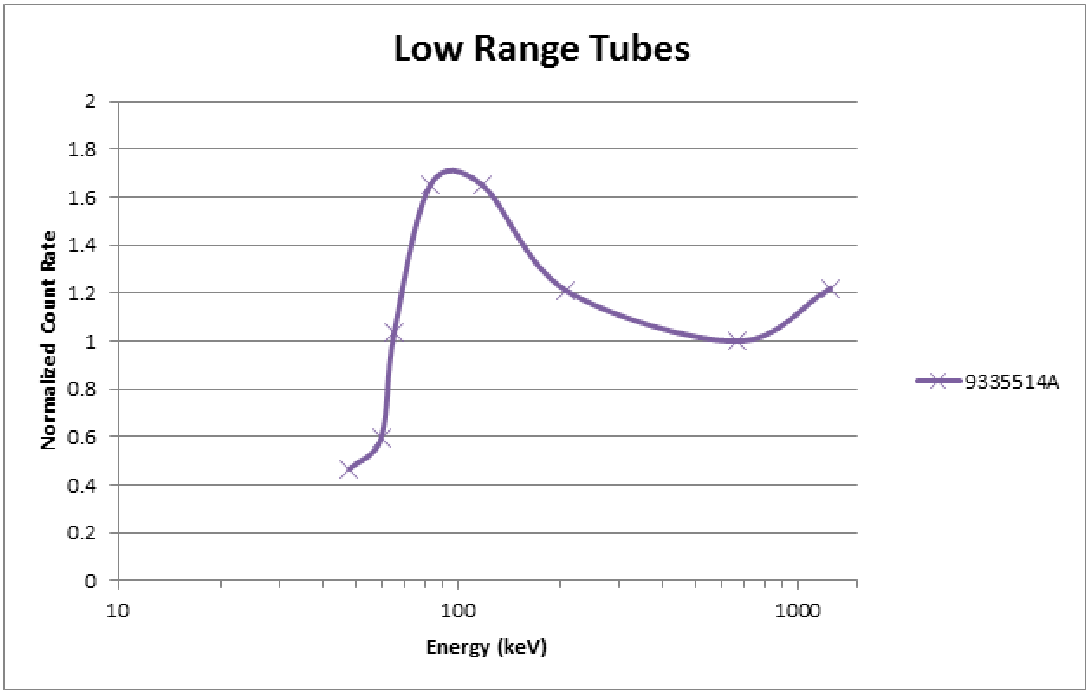

Figure 5: Energy response curve for the low range GM tube in the ADM-300 (Reproduced with permission from* Mirion ®. *See Appendix N.)

.

[2] Mirion ® is a trademark of Mirion Technologies and/or its affiliates in the United States and other countries

Figure 6 shows the energy response curve for the high range tube.

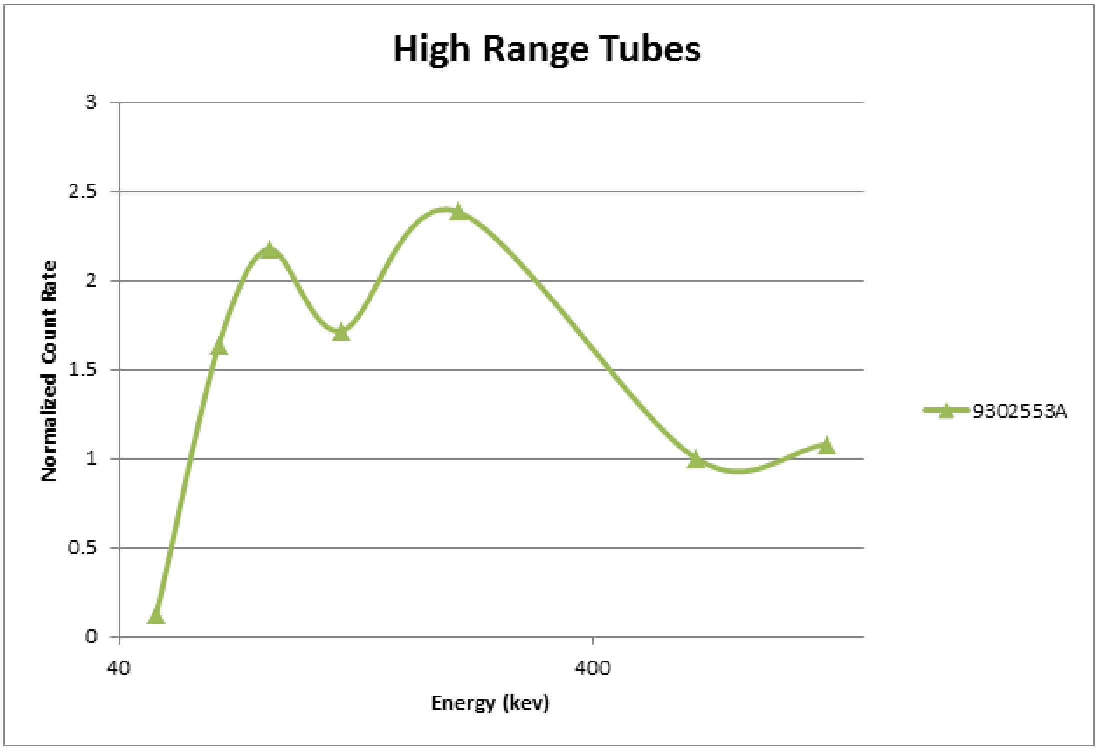

Figure 6: Energy response curve for the high range GM tube in the ADM-300 (Reproduced with permission from* Mirion ®*. See Appendix N.)

Table 8 contains the corrected energy deposition values, as well as the measurement to model ratios and the associated percent differences. The corrected MCNP values were extrapolated from the low range and high range energy response curves.

Table 8: Comparison of net measured values versus MCNP energy response corrected values for the ADM-300.

Radionuclide	Net Measured Value [R/hr]	Corrected MCNP Value [R/hr]	Measurement/MCNP	Percent Difference
Am-241	N/A	N/A	N/A	N/A
Ba-133	1.48E-04	5.25E-04	0.28	-71.87
Co-60	1.28E-03	5.75E-04	2.22	122.26
Cs-137	3.45E-04	3.45E-04	1.00	0.00
Mn-54	2.90E-05	1.57E-05	1.85	85.14

The model was not validated to the desired level due to the lack of information provided and the assumptions that were necessary to complete the model.

Collisional stopping power calculations were performed for the high energy range tube and the low energy range tube and are shown in Appendix K and Appendix L, respectively. The muon and anti-muon weighted average stopping powers for each energy per tube were summed and normalized to result in a total weighted average collisional stopping power. The stopping powers for the active volumes of the high energy range and low energy range GM tubes were theoretically calculated at about 2.29×10^{-3} MeV cm^{-1} and 6.26×10^{-4} MeV cm^{-1}, respectively. The average chord length for the high energy range tube was about 0.29 cm (0.114 in), and the average chord length for the low energy range tube was about 1.55 cm (0.61 in). The stopping power for each tube was multiplied by the corresponding average chord length to result in theoretical average energy depositions of 0.663 keV for the high range tube and 0.968 keV for the low range tube. Therefore, the total average energy deposition within the active volumes of the detector was 1.63 keV.

The theoretical average energy deposition was then compared to energy deposition from the muon and anti-muon MCNP simulations. The energy deposition from the muon simulation in the high range tube was 2.71×10^{-11} MeV and 4.45×10^{-11} MeV for the anti muon simulation. Therefore, the total energy deposition due to muons and anti-muons in the high range tube was

7.16×10^{-11} MeV. The energy deposition in the low range tube was 9.56×10^{-10} MeV and 1.17×10^{-9} MeV for the muon and anti-muon simulations, respectively. The total energy deposition in the low range tube was 2.13×10^{-9} MeV. Therefore, the total energy deposition due to muons and anti-muons in both internal GM tubes was 2.20×10^{-9} MeV based on the MCNP simulations.

The average background measurement, 3.30×10^{-5} R h^{-1} was divided by the estimated fluence to exposure rate conversion, 4.02×10^{-7} R h^{-1} per particle cm^{-2} s^{-1} resulting in 82.05 particle cm^{-2} s^{-1}. The fluence rate was then multiplied by the combined cross-sectional areas of the two GM tubes, 7.599 cm^{2}, resulting in 582.5 particles s^{-1} that pass through the total active volume of the detector due to background. Based on the assumption stated previously, the detector fires about 582.5 times per second due to background radiation. The fluence rate calculated from anti-muons was 0.129 particles cm^{-2} s^{-1} and 0.117 particles cm^{-2} s^{-1} from muons. Thus, the total combined fluence rate was 0.246 particles cm^{-2} s^{-1}. Therefore, the total number of muons and anti-muons that pass through the active volumes of the detector per second was calculated at about 1.75 particles s^{-1}. The percent contribution of muons and anti-muons to the background measurement was 0.3 percent, resulting in a measured exposure rate of 99 nR h^{-1}, assuming every muon and anti-muon passing through the detector results in a detectible ionization. The contribution of muons and anti-muons for the background measurement is negligible and is not the primary cause of the exposure rate discrepancy between the two detectors.

Discussion

451P Pressurized Ionization Chamber

If the data collection experiment was repeated again, the source would be located at least 2.54 cm (1 in) away from the white dot located on the side of the detector to ensure it is represented as a point source. Also, filters with appropriate thickness would be placed in between the source and the detector to block all of the beta particles and cascade electrons.

The energy response correction improved the percent difference for every radionuclide except Am-241. The measured values obtained from the radionuclides, Co-60, Cs-137, and Mn-54 are in good agreement with the MCNP model. Each of the measured values was within 7 percent of the MCNP result, which is acceptable due to the ±20 percent calibration factor of the detector. The deviation between the measurements and models for Ba-133 and Am-241 may be attributed to the fact that energy deposition was greatest at energies were the detector response was not unity. The MCNP results for energy deposition were larger than the measured values of the detector for all sources except Am-241. The total energy deposition from the simulations for Am-241 could have been slightly increased if all 109 photons within the energy response limits of the detector were simulated instead of only 24 photons. The added energy deposition would slightly reduce the measurement to MCNP ratio, resulting in a decreased percent difference.

More accurate results could have been obtained if the engineering documents for the detector were provided by Fluke Biomedical. Constructing the model as a realistic (non-simplified) representation of the detector may have improved the results by accounting for scattering, attenuation, and other interactions with matter inside the detector.

The calculated energy deposition due to muons and anti-muons was almost five orders of magnitude larger than the MCNP energy deposition result. The discrepancy is believed to be due to inaccurate source definitions for the muon and anti-muon input files for MCNP. The muon and anti-muon source may be better represented utilizing Lawrence Livermore National Laboratory's cosmic-ray shower library (CRY). The CRY library can be called from the MCNP input deck allowing software to generate correlated cosmic-ray particle shower distributions at the following three different elevations: sea level, 2100 meters (6890 ft), and 11,300 meters (37,073 ft). The user can further define specific latitudes and dates. (Hagmann, 2012)

An absorbed dose of 2×10^{-16} Gy per muon and anti-muon and an exposure of 1.72×10^{-14} R per muon and anti-muon were determined from the MCNP energy deposition of 2.91 eV. The exposure rates calculated from the MCNP total average energy deposition result using the horizontal and vertical cross-sectional areas of the chamber were 0.337 nR h^{-1} and 0.835 nR h^{-1} for both muons and anti-muons. The 92 keV energy deposition equates to an absorbed dose of 6.33 pGy per muon and anti-muon and an exposure of 0.544 nR per muon and anti-muon. The exposure rates calculated from the average energy deposition that was theoretically calculated were based on the horizontal and vertical cross-sectional areas were 10.7 μR h^{-1} and 26.4 μR h^{-1} for muons and anti-muons. The exposure rate calculated using the horizontal cross-sectional area underestimates the true exposure rate and the exposure rate calculated using the vertical cross-sectional area overestimates the true exposure rate, assuming the calculated combined muon and anti-muon fluence rate and energy deposition are correct. The exposure rates calculated based on the theoretical energy deposition calculation and MCNP energy deposition result due to muons were compared to values obtained from NCRP report 160 *Ionizing Radiation Exposure of the Population of the United States* and *Overview of Aircraft Radiation Exposure* *and Recent Er-2 Measurement* to benchmark the results. (NCRP, 2009) (Goldhagen, 2000) From NCRP Report 160, the average annual effective dose outdoors from space radiation was 0.82 mSv in Colorado Springs. The radiation weighting factor used for space radiation was 2. Therefore, 0.82 mSv yr^{-1} was divided by 2 and was converted into an exposure rate of 4.03 μR h^{-1} using methodology from ICRU 10b. The exposure rate was then multiplied by 0.8 which is the factor NCRP uses to obtain indoor values. A value of 3.22 μR h^{-1} was calculated as an indoor exposure rate due to all space radiation averaged over an 11 year solar cycle. Then total effective dose rates were extrapolated from Figure 1 in *Overview of Aircraft Radiation Exposure and Recent Er-2 Measurement* to obtain values for total space radiation and muon radiation at 1524 m (5,000 ft). Goldhagen's data in the figure was collected at the edge of the polar plateau during minimum solar activity. The effective dose rate due to muon was divided by the total effective dose rate from space radiation to determine the muon contribution of the dose rate. About 52 percent of the effective dose rate from space radiation is due to muons. The muon contribution to the total space radiation was then multiplied by the NCRP 160 value and the effective dose rate from muons at 1524 m (5,000 ft) was converted into an exposure rate. The expected exposure rate due to muons where the experimental data was collected should be between about 1.55 μR h^{-1} to 1.68 μR h^{-1}. Therefore, exposure rates based on the MCNP simulations underestimated the value, and exposure rates based on the theoretical calculation were an over-estimate. A summary of the values obtained from the MCNP results and calculated results, as well as the expected values from NCRP 160 and Goldhagen are shown in Table 9.

Table 9: Summary of the simulated MCNP values, calculated values, and expected values for exposure rates due to muons and anti-muons for the 451P pressurized ionization chamber.

Method	Energy Deposition [keV]	Absorbed Dose [Gy/particle]	Exposure [R/particle]	Exposure Rate Range [µR/ hr]
MCNP	2.91E-03	2.00E-16	1.72E-14	0.337E-3 - 0.835E-3
Calculated	92	6.33E-12	5.44E-10	10.7 - 26.4
NCRP/GoldHagen	-	-	-	1.55 - 1.68

The Bethe-Bloch formula could have been used to provide a more accurate calculation of the theoretical stopping power. The Bethe-Bloch formula is similar to the Bethe equation but includes quantum-mechanical correction factors to calculate stopping power. The Bethe-Bloch formula includes density effects and shell correction effects.

ADM-300

The energy response correction for the low range tube improved the percent difference for Co-60 and Mn-54 slightly, however the correction for Ba-133 made the model worse. Above 80 keV (detection limit) the low range tube over responds, therefore the multiplicative factor correcting the MCNP value is greater than 1. Since the uncorrected MCNP value for Ba-133 was already larger than the measured value, the energy response correction further deviates the model from the measurement. The energy response curve for the high range tube is even further from unity then the low range tube response. The high range tube over responds to energies between about 80 keV and 660 keV and under responds to energies between about 700 keV to about 1100 keV. After adjustments were made for the energy response in both tubes, the percent difference between the measurement and the model for Ba-133 and Mn-54 increased, and the result for Co-60 was improved. The result for Cs-137 was unaffected since the detector was calibrated to Cs-137 and therefore, energy response should be one.

The calculated energy deposition and the MCNP energy deposition results varied greatly. The difference in energy deposition in the high range tube was of about 7 orders of magnitude and the difference in energy deposition in the low range tube was about 5 orders of magnitude. The total energy deposition difference in both tubes was about 6 orders of magnitude. In all cases, the MCNP value was significantly smaller. The calculated total energy deposition of 1.63 keV seems more realistic than the MCNP result of 2.20×10^{-6} keV.

Based on the theoretically calculated energy deposition, enough energy is deposited in the tube to cause ionizations resulting in a Geiger discharge, causing the detector to send a signal. Therefore, the contribution of muons and anti-muons in the background measurement needs to be determined in order to see if the contribution is significant or negligible. Since the percent contribution of muons and anti-muons to the background measurement was only 0.3 percent, the measured exposure rate registered in the GM was only 99 nR h^{-1}. The calculated exposure rate registered in the GM were still well below the expected range of 1.55 μR h^{-1} and 1.68 μR h^{-1} as determined by NCRP 160 and Goldhagen. Regardless, the calculated contribution of muons and anti-muons for the background measurement is negligible and is not the primary cause of the exposure rate discrepancy between the two detectors.

The MCNP model for the ADM-300 could have been improved if more information was provided. Specifically, information on the true fluence rate to exposure rate conversion for the detector is needed. All results for the ADM-300, except for the stopping power were based on the estimated conversion, potentially impacting the results if the estimate was not correct. Similar to the pressurized ionization chamber, using the CRY library for the muon source could provide a more representative model possibly increasing the energy deposition in the detector, making the MCNP model closer to calculated energy deposition.

Conclusion

The exposure rate due to muons and anti-muons for the 451P pressurized ionization chamber was between 10.7 $\mu R\ h^{-1}$ and 26 $\mu R\ h^{-1}$ based on the calculation using the theoretical stopping power, the average chord length, and the muon and anti-muon fluence rate. The exposure rate based on the MCNP simulations was between 0.337 $nR\ h^{-1}$ and 0.835 $nR\ h^{-1}$. The exposure rate registered in the ADM-300 energy compensated GM was 99 $nR\ h^{-1}$ based on the estimated fluence rate to exposure rate, the background measurement value, and the muon and anti-muon fluence rate.

Due to the difficulty of obtaining the detectors, measurements were made at different times. If the experiment was performed again, it would be beneficial to have both detectors at the same time of measurement, allowing the user to observe if the discrepancy existed during actual source measurements, instead of exposure rates due to background at different times. Both detectors should also be calibrated at the same place by the same company to minimize any calibration factors influencing the measurements.

From the energy deposition calculation and the simulated results, more energy was deposited in the active volume of the pressurized ionization chamber than the energy compensated GM tubes. Theoretically, more energy should be deposited in the pressurized ionization chamber due to the active volume being over 5 times larger than the active volumes of the energy compensated GM tubes combined. Furthermore, the ion chamber is at a higher pressure than the high and low range GM tubes. The higher pressurize at a fixed volume increases the movement of the atoms within the chamber resulting in a higher probability of interaction.

The use of a cosmic veto system for both detectors would be a valuable way to discriminate the background exposure rates to muons and further characterize the discrepancy. Cosmic veto systems utilize anti-coincidence logic that can eliminate much of the cosmic contribution to background. Cosmic veto background reduction systems suppress cosmic radiation as much as 15 to 40 percent resulting in lower minimum detectable activities and count times. (Cosmic, 2016)

The cause of the exposure rate discrepancy between the pressurized ionization chamber and the energy compensated GM tubes was not due to muon and anti-muon cosmic particles. The cause of the discrepancy is still unknown and further research must be performed in order to characterize the discrepancy. Possible future studies may include investigation of other cosmic particles and waves influencing the exposure rate. Also, investigating detector response due to terrestrial radiations, such as thorium and uranium decay series and K-40 to see if the energy compensated GM tubes over-respond. Measurements also need to be obtained in a higher exposure radiation field to see if the exposure rate discrepancy still exists or if the discrepancy in background exposure rate measurements is negligible. In addition, the electronic rejection of the detector should be taken into consideration to further classify the contribution of muons to the measured background exposure rate.

Care should be taken when using energy compensated GM tubes to evaluate dose or exposure rates. The energy response curves for tubes were far from unity, with a maximum value of almost 2.4. The response curves and the constituents of the radiation field must be considered when using this instrument for exposure rates. Until the discrepancy is characterized or if it is determined to be negligible in a higher radiation field, it is recommended energy compensated GM tubes should only be used in a single source environment, for which the detector is calibrated. Pressurized ionization chambers are still the golden standard to measure radiation dose or exposure.

References

ADM - 300 Multi-Functional Survey Instrument. (n.d.). Retrieved May 25, 2017, from https://www.southernscientific.co.uk/data/file/0/b/Canberra_ADM300_DEC.1438855616.pdf

Amsler, C. (2010, February 2). PASSAGE OF PARTICLES THROUGH MATTER. Retrieved March 16, 2017, from http://pdg.lbl.gov/2009/reviews/rpp2009-rev-passage-particles-matter.pdf

Borak, T. B. (1994). A Method for Computing Random Chord Length Distributions in Geometrical Objects. *Radiation Research,137*(3), 346. doi:10.2307/3578709

Brandl, A. (2015). *Alpha Range and Energy Transfer*. Lecture presented at Colorado State University in Colorado, Fort Collins.

Brey, R. R. (n.d.). *Radiation Physics (54-330)* (N. Fallahian, Ed.).

Cember, H., & Johnson, T. E. (2009). *Introduction to Health Physics* (4th ed.). New York: McGraw-Hill.

Cosmic Veto Background Reduction System. (2016, June). Retrieved June 12, 2017, from http://www.canberra.com/products/detectors/pdf/CosmicGuard-C48953.pdf

Eckerman, K. F., Westfall, R. J., Ryman, J. C., & Cristy, M. (1994). Availability of nuclear decay data in electronic form, including beta spectra not previously published. Health Physics, 67(4), 338-345.

Fluke Biomedical. (2013). *451P Ion Chamber Survey Meter: Operators Manual*. Retrieved October 16, 2016, from http://assets.fluke.com/manuals/451P____omeng0100.pdf

Gaisser, T. K. (1990). *Cosmic Rays and Particle Physics*. Cambridge : Cambridge University Press.

Goldhagen, P. (2000). Overview Of Aircraft Radiation Exposure And Recent Er-2 Measurements. *Health Physics,79*(5), 526-544. doi:10.1097/00004032-200011000-00009

Hagmann, C., Lange, D., Verbeke, J., & Wright, D. (2012, March 24). Cosmic-ray Shower Library (CRY). Retrieved June 7, 2017, from https://nuclear.llnl.gov/simulation/doc_cry_v1.7/cry.pdf

Heinrich, W., Roesler, S., & Schraube, H. (1999). Physics of Cosmic Radiation Fields. *Radiation Protection Dosimetry,86*(4), 253-258. doi:10.1093/oxfordjournals.rpd.a032953

ICRU Report 10b Physical Aspects of Irradiation. (1962). *Journal of the ICRU,85*, 2-2. Retrieved June 6, 2017.

ICRU REPORT 84 Reference Data for the Validation of Doses from Cosmic-Radiation Exposure of Aircraft Crew. (2010). *Journal of the ICRU,10*(2). doi:10.1093/jicru/10.2.report84

Knoll, G. F. (2012). *Radiation Detection and Measurement* (4th ed.). Hoboken, NJ: John Wiley & Sons, Inc.

Kremer, J., et al. (1999). Measurements of Ground-Level Muons at Two Geomagnetic Locations. Physical Review Letters, 83(21), 4241-4244.

McConn Jr, R.J. et al. (2011). *Compendium of Material Composition Data for Radiation Transport Modeling*. Richland, WA: Pacific Northwest National Laboratory.

Minerals.net. (n.d.). Retrieved April 25, 2017, from http://www.minerals.net/mineral/muscovite.aspx

NCRP Report No. 160: Ionizing Radiation Exposure of the Population of the United States. (2009). *Recommendations of the NATIONAL COUNCIL ON RADIATION PROTECTION AND MEASUREMENTS*, 31-32. doi:10.1088/0031-9155/55/20/6327

NNDC. (2015). Chart of Nuclides. Retrieved from National Nuclear Data Center: http://www.nndc.bnl.gov/chart/

Point sources. (2016, November 23). Retrieved April 04, 2017, from http://www.ezag.com/home/products/isotope_products/isotrak_calibration_sources/reference_sources/gamma_sources/point_sources/

Rademacher, S. (2015, April 3). *Cosmic Radiation & Issues Surrounding Measurement of Ambient Radiation during Operation Tomodachi*. Lecture presented at Colorado State University in Colorado, Fort Collins.

Serway, R. A., Moses, C. J., & Moyer, C. A. (2005). *Modern physics* (3rd ed.). Belmont, CA: Thomson Brooks/Cole.

Goorley, T. (2012) et al., Initial MCNP6 Release Overview. *Nuclear Technology*, *180*, 298-315

Turner, J. E. (2007). *Atoms, Radiation, and Radiation Protection* (3rd ed.). Weinheim: Wiley-VCH.

U.S. Standard Atmosphere. (n.d.). Retrieved April 04, 2017, from http://www.engineeringtoolbox.com/standard-atmosphere-d_604.html

Appendix A: Calibration Spreadsheet for the Fluke Biomedical 451P-RYR Pressurized Ionization Chamber

Date: November 17, 2016 — Temperature: 21 °C

ION CHAMBER - CALIBRATION REPORT

Instrument: MFR: victoreen fluke — Model # 451 — S/N: 4337

CHAMBER TYPE: ☐ VENTED ☑ PRESSURIZED (PIC) ☐ OTHER

Belongs to: Kraft, Susan — Location: 0555-159

Contamination check: Instrument: ☑ None/OK

Battery Check ? ☑

Meter zero check: Mech: ☑ OK Elec: ☑ OK — Dessicant regenerated ☑ No/OK as is ☐ Yes ☐ None

Repairs/maintenance performed: Performed by Antonio Serpa

Calibration source used: J.L. Shepherd model 28-8B "calibrator" Serial #: 10129 Nuclide: ^{137}Cs

Assay Act: 1009.87596 mCi — Assay Date: 7/22/1998

Calib. Date: 1/1/2008 — Elap Time: 9.452054795 y — Calib. Act: 812.7883 mCi

Current Date : 11/17/2016 *Automatically Updates (Do not adjust)*

Elapsed Time (years): 18.33848481 *Automatically Updates (Do not adjust)*

Date of calculation of exposure rates: Activity on this date: 662.7188 mCi

Correction Factor: 0.8154

digital display

GEOTROPISM TEST **Range tested:**

☐ Source ☐ Pulser ☐ Pass ☐ Fail

Instrument orientation	Reading	% deviation from Vert. Horiz. orientation	Limit:
	40000	Reference	Maximum deviation for each reading: ± 6% of the reference orientation.
Vertical, meter ↑	40000	0.00	
Vertical, meter →	40000	0.00	
Vertical, meter ←	40000	0.00	

REPRODUCIBILITY CHECK Using Source

☑ Pass ☐ Fail

Trial	Reading	Percent deviation from	Limit: Each +/- 10% of the mean
1	4000	0.00	
2	4000	0.00	
3	4000	0.00	
4	4000	0.00	
mean:	4000		

Geometry: Beam incident to detector ☑ Side ☐ Front ☐ Bottom

Equilibrium Cap (or slide) ☐ In place/slide closed ☐ Removed/slide open ☐ N/A (no cap or slide)

γ CALIBRATION DATA Meter readout: Response used: Slow 0.1,X 1 Fast: X 10, X 100

Distance [m]	Atten.	Background (range used)	Reading As Found	Reading Range	Reading As Returned	Net reading As Found	Actual Exposure Rate As Returned	[mR/h]	% error, or CPM C/s = 1 mR/h as found	as ret.
0.5	none	0				0		821.89		
0.75	none	0	0			0		361.45		
1	none	0	170			0		205.31	17	
1.5	none	0				0		92.38		
2	none	0	44			0		53.30	17	
2.5	none	0				0		34.47		
3	none	0	20			0		24.00	17	
2	x4	0				0		12.03		
2.5	x4	0				0		7.79		
3	x4	0	4.8			0		5.42	11	
2.25	x10	0				0		3.86		
* 3.00	x10	0.025	1.95			0		2.19	11	
1.5	x100	0.025	0.72			0		0.83	14	
2.5	x100	0.025	0.27			0		0.30	11	
3	x100	0	0			0		0.21		
1.5	x1000	0.025	0.089			0		0.08	10	
2.5	x1000	0.025	0.044			0		0.03	50	

Integrate Mode Calibration Does this instrument have Mode Capability ☐ Yes ☐ No

Meter Range (x1,x10)	Dist (m)	Attenuation	Exposure Time (min)	Actual Exposure Rate (mR/hr)	Total Actual Exposure (mR)	Indicated Exposure Integ. Mode (mR)	% Error < 10 % ?
	1	None	10	205.31	34.2	26	24
	1.5	None	2	92.38	3.1		
	2	None	5	53.30	4.4	n/a	#VALUE!
	2.5	x4	5	7.79	0.6	n/a	#VALUE!
	3	x4	5	5.42	0.5	n/a	#VALUE!
	2	x4	10	12.03	2.0	n/a	#VALUE!

Within ± 10% : 20% up to 205 mR/hr

Note: Calibration not tested above: 205 mR/hr

mR/hr; range(s) not tested/ calibrated:

Check Source Reading: ☑ No check source

This unit Passes ☑ OK ☐ Failes this calibration

Calibration date: 17-Nov-16 By: A. Serpa Next Cal due: 17-May-17

*** The detector was calibrated at CSU by Antonio Serpa within ± 20 percent of the true value up to 205 mR/h.**

Appendix B: Simulated Radiation for each Radionuclide for the Fluke Biomedical 451P-RYR Pressurized Ionization Chamber

Table B.1.1: Photons simulated for Cs-137.

Emission Type	Energy [keV]	Intensity
XR kα2	31.817	0.0199
XR kα1	32.194	0.0364
XR kβ3	36.304	0.00348
XR kβ1	36.378	0.00672
XR Kβ2	37.255	0.00213
γ1	283.5	5.8E-06
γ2	661.657	0.851

Table B.1.2: Beta distribution simulated for Cs-137.

137CS B- DECAY (30.04 Y 3)					
Reference 1					
Energy	**Bi**	**n (MeV)**	**#/beta transition**	**Energy (MeV)**	**#/nt**
				Average	
0.0000	-	0.0587	1.93E-01	0.0294	1.93E-01
0.0587	-	0.1173	1.76E-01	0.0880	1.76E-01
0.1173	-	0.1760	1.61E-01	0.1467	1.61E-01
0.1760	-	0.2346	1.44E-01	0.2053	1.43E-01
0.2346	-	0.2933	1.22E-01	0.2640	1.22E-01
0.2933	-	0.3520	9.38E-02	0.3227	9.38E-02
0.3520	-	0.4106	6.01E-02	0.3813	6.01E-02
0.4106	-	0.4693	2.64E-02	0.4400	2.64E-02
0.4693	-	0.5279	5.70E-03	0.4986	5.70E-03
0.5279	-	0.5866	3.31E-03	0.5573	3.30E-03
0.5866	-	0.6453	3.08E-03	0.6160	3.07E-03
0.6453	-	0.7039	2.83E-03	0.6746	2.82E-03
0.7039	-	0.7626	2.54E-03	0.7333	2.53E-03
0.7626	-	0.8212	2.20E-03	0.7919	2.20E-03
0.8212	-	0.8799	1.83E-03	0.8506	1.83E-03
0.8799	-	0.9386	1.42E-03	0.9093	1.42E-03
0.9386	-	0.9972	9.92E-04	0.9679	9.92E-04
0.9972	-	1.0559	5.91E-04	1.0266	5.91E-04
1.0559	-	1.1145	2.45E-04	1.0852	2.45E-04
1.1145	-	1.1732	5.38E-05	1.1439	5.38E-05

Appendix B (continued)

Table B.2.1: Photons simulated for Co-60.

Emission Type	Energy [keV]	Intensity
$\gamma 1$	347.14	0.000075
$\gamma 2$	826.1	0.000076
$\gamma 3$	1173.228	0.9985
$\gamma 4$	1332.492	0.999826
$\gamma 5$	2158.57	0.000012
$\gamma 6$	2505.692	2E-08

Table B.2.2: Beta distribution simulated for Co-60.

60CO B- DECAY (1925.3 D3)					
Reference 1					
Energy	**Bi**	**n (MeV)**	**#/beta transition**	**Energy (Mev)**	**#/nt**
				Average	
0.0000	-	0.0746	4.45E-01	0.0373	4.45E-01
0.0746	-	0.1491	3.30E-01	0.1119	3.30E-01
0.1491	-	0.2237	1.78E-01	0.1864	1.78E-01
0.2237	-	0.2982	4.58E-02	0.2610	4.58E-02
0.2982	-	0.3728	6.36E-04	0.3355	6.36E-04
0.3728	-	0.4473	5.99E-05	0.4101	5.99E-05
0.4473	-	0.5219	5.96E-05	0.4846	5.96E-05
0.5219	-	0.5964	5.77E-05	0.5592	5.77E-05
0.5964	-	0.6710	5.54E-05	0.6337	5.54E-05
0.6710	-	0.7455	5.40E-05	0.7083	5.40E-05
0.7455	-	0.8201	5.23E-05	0.7828	5.23E-05
0.8201	-	0.8947	4.99E-05	0.8574	4.99E-05
0.8947	-	0.9692	4.66E-05	0.9320	4.66E-05
0.9692	-	1.0438	4.24E-05	1.0065	4.24E-05
1.0438	-	1.1183	3.71E-05	1.0811	3.71E-05
1.1183	-	1.1929	3.06E-05	1.1556	3.06E-05
1.1929	-	1.2674	2.31E-05	1.2302	2.31E-05
1.2674	-	1.3420	1.47E-05	1.3047	1.47E-05
1.3420	-	1.4165	6.66E-06	1.3793	6.66E-06
1.4165	-	1.4911	1.57E-06	1.4538	1.57E-06

Appendix B (continued)

Table B.2.3: Cascade electrons simulated for Co-60

Emission Type	Energy [keV]	Intensity
CE k	1164.895	1.50E-04
CE L	1172.22	1.46E-05
CE N	1173.228	8.87E-08
CE M	1173.228	2.06E-06
CE K	1324.159	1.14E-04
CE L	1331.484	1.11E-05
CE M	1332.492	1.56E-06
CE N	1332.492	6.73E-08
CE K	2150.24	5.30E-10
CE L	2157.56	5.20E-11
CE M	2158.57	7.30E-12
CE N	2158.57	3.20E-13
CE K	2497.359	1.60E-12
CE L	2504.684	1.50E-13
CE M	2505.692	2.10E-14
CE N	2505.692	9.20E-16

Table B.3.1: Photons simulated for Ba-133

Emission Type	Energy [keV]	Intensity
XR kα2	30.625	0.339
XR kα1	30.973	0.622
XR kβ3	34.92	0.0588
XR kβ1	34.987	0.114
XR kβ2	35.818	0.0351
γ1	53.1622	0.0214
γ2	79.6142	0.0265
γ3	80.9979	0.329
γ4	160.612	0.00638
γ5	223.2368	0.00453
γ6	276.3989	0.0719
γ7	302.8508	0.1834
γ8	356.0129	0.6205
γ9	383.8485	0.0894

Appendix B (continued)

Table B.4.1: Photons simulated for Mn-54

Emission Type	Energy [keV]	Intensity
Annihilation	511	6.00E-09
γ1	834.848	0.99976

Table B.5.1: Photons simulated for Am-241

Emission Type	Energy	Intensity
γ1	26.3446	0.0227
γ2	33.196	0.00126
γ3	42.704	0.000055
γ4	43.42	0.00073
γ5	55.56	0.000181
γ6	59.5409	0.359
γ7	64.83	1.45E-06
γ8	67.45	4.2E-06
γ9	69.76	0.000029
γ10	75.8	5.9E-06
XR kα2	97.069	1.14E-05
γ11	98.97	0.000203
XR kα1	101.059	1.81E-05
γ12	102.98	0.000195
XR kβ3	113.303	2.27E-06
XR kβ1	114.234	2.43E-05
XR kβ2	117.463	1.68E-06
γ13	123.052	0.00001
γ14	125.3	4.08E-05
γ15	146.55	4.61E-06
γ16	169.56	1.73E-06
γ17	208.01	7.91E-06
γ18	322.52	1.52E-06
γ19	332.35	1.49E-06
γ20	335.37	4.96E-06
γ21	368.65	2.17E-06
γ22	376.65	1.38E-06
γ23	662.4	3.64E-06
γ24	722.01	1.96E-06

Appendix C: Beta Input File Example for the Fluke Biomedical 451P – RYR Pressurized Ionization Chamber

```
C Fluke Biomedical PIC MODEL 451P--11/17/2016
c Measurement validation
c Source: Cs-137 w/ Activity: 1.738E5 Disc (Type D) source on surface of detector case
C Beta Simulation
<<<<<<<<<<<<<<<<<<<<<<<<<<<<<<<<CELLs>>>>>>>>>>>>>>>>>>>>>>>>>>>>>>
C
1    3 -0.0102 -1                 IMP:P=16 IMP:E=16 $ ACTIVE CHAMBER VOLUME
2    2 -0.281215 1 -2             IMP:P=8 IMP:E=8    $ CHAMBER WALL
3    1 -1.05698E-3 2 -3           IMP:P=4 IMP:E=4    $ AIR BETWEEN CASE AND CHAMBER
4    4 -0.930 3 -4                IMP:P=2 IMP:E=2    $ CASE WALL
5    1 -1.05698E-3 4 5 -999  IMP:P=1 IMP:E=1    $ AIR OUTSIDE CASE
6    4 -0.930 -5                  IMP:P=1 IMP:E=1    $ PLASTIC SOURCE HOUSING
900    0 999                      IMP:P=0 IMP:E=0    $ OUTSIDE UNIVERSE

C
<><><><><><><><><><><><><><><<SURFACES><><><><><><><><><><><><><><>
>
C
1     RCC 0 0 -5.1562 0 0 10.3124 2.6543                      $ INNER CHAMBER
2     RCC 0 0 -5.8674 0 0 11.7348 3.3655                      $ OUTER CHAMBER WALL
3     RPP -6.1976 13.4976 -4.8476 4.8476 -7.1514 7.5438  $ INNER CASE WALL
4     RPP -6.35 13.65 -5 5 -7.3038 7.6962                     $ OUTER CASE WALL
5     RCC 0 -5 0 0 -0.635 0 1.27                              $ Plastic Source Housing
999   SO 900                                                  $ UNIVERSE

C ################################# DATA ##################################
C
C __________________________________ Materials ______________________________
C
c    AIR, PHOTON, Dry air at 5000' interpolated from engineeringtoolbox.com
M1    6000.  -0.000124
      7000.  -0.755268           $ DENSITY = 1.05698E-3 [G/CM3]
      8000.  -0.231781
     18000.  -0.012827
c
c    POLYETHYLENE, NON-BORATED (USED AS PLASTIC)    FOR CHAMBER WALL
M2    1000.  -0.143716           $ CALULATED DENSITY FROM MANUAL = 0.281215
      6000.  -0.856284
c
c    NITROGEN / ARGON MIX
M3    7000.   0.955  $ NITROGEN  CALULATED DENSITY & pressure corrected:0.0102
      18000.  0.045  $ ARGON
```

```
C
c     POLYETHYLENE, NON-BORATED (USED AS PLASTIC)    FOR CASE WALL
M4    1000.  -0.143716            $ DENSITY = 0.930 [G/CM3]
        6000.  -0.856284
C
C ______________________________ SOURCE DEFINITION __________________________
C
SDEF POS= 0 -5.595 0 AXS= 0 1 0 RAD= D1 EXT= d2 PAR= E &
 ERG= d3                              $ button SOURCE on side dot of detector
SI1 0 0.25
SP1 -21 1
si2 0 0.318
sp2 -21 0
si3  H 0 2.94E-02 8.80E-02 1.47E-01 2.05E-01 2.64E-01 3.23E-01 3.81E-01 &
     4.40E-01 4.99E-01 5.57E-01 6.16E-01 6.75E-01 7.33E-01 7.92E-01 &
     8.51E-01 9.09E-01 9.68E-01 1.03E+00 1.09E+00 1.14E+00
sp3   0 1.93E-01 1.76E-01 1.61E-01 1.43E-01 1.22E-01 9.38E-02 6.01E-02 &
     2.64E-02 5.70E-03 3.30E-03 3.07E-03 2.82E-03 2.53E-03 2.20E-03 &
     1.83E-03 1.42E-03 9.92E-04 5.91E-04 2.45E-04 5.38E-05
C
C ________________________________ TALLY_______________________________________
C
*F8:P,E 1                              $ ENERGY DEPOSITION CHAMBER VOLUME [MeV]
NPS 1E8
MODE P E
```

Appendix D: Muon Input File Example for Fluke Biomedical 451P – RYR Pressurized Ionization Chamber

```
C Fluke Biomedical PIC MODEL 451P--3/10/2017
c Cosmic Muon Source --SPHERE SOURCE
c Muons Energy Dist/Intensity based off of 1270m (4166.67ft)
c
C
<<<<<<<<<<<<<<<<<<<<<<<<<<<<<<<<<CELLS>>>>>>>>>>>>>>>>>>>>>>>>>>>>>>
C
1    3 -0.0102 -1               Imp:|=16 imp:p=16 $ ACTIVE CHAMBER VOLUME
2    2 -0.281215 1 -2           Imp:|=8 imp:p=8    $ CHAMBER WALL
3    1 -1.05698E-3 2 -3         Imp:|=4 imp:p=4    $ AIR BETWEEN CASE AND CHAMBER
4    4 -0.930 3 -4              Imp:|=2 imp:p=2    $ CASE WALL
5    1 -1.05698E-3 4 -999       Imp:|=1 imp:p=1    $ AIR OUTSIDE CASE
6    0 999                      Imp:|=0 imp:p=0    $ OUTSIDE UNIVERSE

C
<><><><><><><><><><><><><><><><SURFACES><><><><><><><><><><><><><><>
C
1     RCC 0 0 -5.1562 0 0 10.3124 2.6543                    $ INNER CHAMBER WALL
2     RCC 0 0 -5.8674 0 0 11.7348 3.3655                    $ OUTER CHAMBER WALL
3     RPP -6.1976 13.4976 -4.8476 4.8476 -7.1514 7.5438   $ INNER CASE WALL
4     RPP -6.35 13.65 -5 5 -7.3038 7.6962                   $ OUTER CASE WALL
999   SO 1000                                               $ Sphere as UNIVERSE

C ################################# DATA ##################################
C
c     AIR, PHOTON, interpolated at 5000' from engineeringtoolbox.com
M1    6000.  -0.000124
    7000.  -0.755268          $ DENSITY = 1.05698E-3 [G/CM3]
    8000.  -0.231781
    18000. -0.012827
c
c     POLYETHYLENE, NON-BORATED (USED AS PLASTIC)    FOR CHAMBER WALL
M2    1000.  -0.143716          $ CALULATED DENSITY FROM MANUAL = 0.281215
       6000.  -0.856284
c
c     NITROGEN / ARGON MIX
M3    7000.   0.955  $ NITROGEN    CALULATED DENSITY & pressure corrected: 0.0102
      18000.  0.045  $ ARGON
C
c     POLYETHYLENE, NON-BORATED (USED AS PLASTIC)    FOR CASE WALL
M4    1000.  -0.143716          $ DENSITY = 0.930 [G/CM3]
       6000.  -0.856284
C
```

```
PHYS:| 5E6
SDEF SUR=999 NRM=-1 erg=d3 PAR= | $ SOURCE ON UNIVERSE SURFACE DIRECTED
INSIDE THE SPHERE
si3  200 300 400 550 700 850 1000 1200 1400 1600 2100 2940 4120 &
    5500 7000 10000 15500 23000 31100 43600 61100 85600 120000
# sp3
     0
     0.067239226
     0.095517406
     0.112484313
     0.116883141
     0.110599102
     0.103058254
     0.09300379
     0.08043571
     0.071638054
     0.057813167
     0.035819027
     0.024256394
     0.014516132
     0.008609135
     0.004901551
     0.002010893
     0.000728949
     0.000282782
     0.000127566
     4.83871E-05
     2.01089E-05
     6.91244E-06
C
*F8:| 1                              $ ENERGY DEPOSITION IN CHAMBER VOLUME [MeV]
NPS 1E9
MODE | p
```

<u>**Appendix E: Certificate of Calibration for the ADM-300 Multi-Functional Survey Meter**</u>

AIR FORCE PRIMARY STANDARDS LABORATORY

CERTIFICATE OF CALIBRATION

Report Number: 163640006 **Department:** Photonics/Nucleonics **Date of Issue:** 20170104

Calibration Item:
Manufacturer: NUCLEAR RESEARCH CORPORATION
Model/Part No.: ADM-300A

Equipment Type: RADIAC METER, MULTI-FUNCTION
Serial Number: ADM-690331
ID Number: C043355

Equipment Submitted by:
GOLDBELT FALCON/PMEL
5104 15th CAVALRY AVE. BLDG 341
SOUTH
F.E. WARREN AFB, WY, 82005-2175

Item Condition:
As Received: IN-TOLERANCE
The measured values of all parameters tested or calibrated were found to be within specification limits.

As Returned: IN-TOLERANCE
Item was calibrated and ALL calibration authority parameters were verified and returned with EACH parameter meeting the calibration authority specifications. The item may or may not have been adjusted. Includes TO directed limitations.

Room Ambient Conditions:
Temperature: 68.34 °F Relative Humidity: 35.8 % Barometric Pressure: N/A

Remarks:

Traceability: Measurement standards and test equipment used are traceable to the International System of Units (SI) through the National Institute of Standards and Technology, to the extent allowed by the Institute's calibration facilities; or to other National Metrology Institutes (NMI); or have been derived from accepted values of natural physical constants; or mutual consent standards; or have been derived by the ratio or reciprocity type measurement techniques.

General Conditions:
1. The standards and calibration program of the AFPSL, as operated by The Bionetics Corporation, Newark Metrology Operations, complies with the requirements of the current version of ISO/IEC 17025 on the date of calibration.
2. This report may not be reproduced, except in full, without written approval of The Bionetics Corporation, Newark Metrology Operations.

Calibrated By:
Mark Cooperrider **Metrology Technician**

AF P 484 S L

Phone: DSN 366-5451
E-mail: Mark.Cooperrider.ctr@us.af.mil

Approved By:
Donald M. Hayes **Lead Metrology Technician**

AF P 483 S L

Phone: (740) 788-5451
E-mail: Donald.Hayes.ctr@us.af.mil

bionetics
VISION • VALUE • INTEGRITY
813 Irving-Wick Drive West, Heath, Ohio 43056-6118 TEL: (740) 788-5400 FAX: (740) 788-5404

Page 1 of 2

Report Number: 163640006
Date of Issue: 20170104
Model/Part No.: ADM-300A
Serial Number: ADM-690331

Procedures and Equipment Used

PROCEDURES

Procedure	**Date**
33K7-4-170-1	28 Feb 2012

EQUIPMENT

Nomenclature	**Model/Part No.**	**ID No.**	**NIST Report No.**	**Cal Due Date**
CESIUM-137 STANDARD	81-10	P71065	N/A	20170410

The reported value(s) and uncertainties resulting from the measurement process are:

Report of Measurement

Applied	T.I. Reading
250 R/hr	258 R/hr
100 R/hr	102 R/hr
25 R/hr	25.6 R/hr
250 mR/hr	252 mR/hr
2 mR/hr	1.97 mR/hr

- The instrument calibration results are accurate to within ±15% of true dose.
- Calibrated for gamma only (T.O. directed limitation).

bionetics
VISION • VALUE • INTEGRITY
813 Irving-Wick Drive West, Heath, Ohio 43056-6118 TEL: (740) 788-5400 FAX: (740) 788-5404

Appendix F: Simulated Radiation for Each Radionuclide for the ADM-300 Multi-Functional Survey Meter

Table F.1: Photons Simulated for Cs-137.

Emission Type	Energy [keV]	Intensity
γ1	283.5	
γ2	661.657	0.851

Table F.2: Photons Simulated for Co-60.

Emission Type	Energy [keV]	Intensity
γ1	347.14	7.5E-05
γ2	826.1	7.6E-05
γ3	1173.228	0.9985
γ4	1332.492	0.99983
γ5	2158.57	1.2E-05
γ6	2505.692	2.00E-08

Table F.3: Photons Simulated for Ba-133.

Emission Type	Energy [keV]	Intensity
γ1	80.9979	0.329
γ2	160.612	0.00638
γ3	223.2368	0.00453
γ4	276.3989	0.0719
γ5	302.8508	0.1834
γ6	356.0129	0.6205
γ7	383.8485	0.0894

Table F.4: Photons Simulated for Mn-54.

Emission Type	Energy [keV]	Intensity
γ1	834.848	0.99976

Appendix G: Exposure Rate Discrepancies between the Ludlum Model D9P pressurized ionization chamber and the ADM-300 Multi-Functional Survey Meter

	ADM-300	Model D9P	
Source	**Net Measurement [R/hr]**	**Net Measurement [R/hr]**	**Percent Difference (ADM-PIC)**
Am-241	N/A	9.46E-06	
Ba-133	1.48E-04	2.22E-04	-33.44735893
Co-60	1.28E-03	6.16E-04	107.3859945
Cs-137	3.45E-04	3.04E-04	13.15858626
Mn-54	2.90E-05	1.81E-05	60.57585825

*** All Dose rate measurements obtained using the Ludlum Model D9P were converted into exposure rates using ICRU 10b methodology.**

*** Measurements taken 1" away from both detectors & at the same time**

Appendix H: Fluke Biomedical 451P – RYR Pressurized Ionization Chamber Photon, Beta, and Cascade Electron MCNP results

Table H.1: Simulated results from the Cs-137 MCNP model.

RadioNuclide	**Activity [Bq]**		Measured Value [R/hr]			
Cs-137	1.74E+05		4.08E-04			
Emission Type	**Energy [keV]**	**Intensity**	**MCNP [MeV/SP]**	**Error**	**MeV/s**	**[R/hr]**
XR kα2	31.817	0.0199	5.61E-05	0.002	1.94E-01	5.58E-06
XR kα1	32.194	0.0364	5.49E-05	0.002	3.47E-01	1.00E-05
XR kβ3	36.304	0.00348	4.39E-05	0.0023	2.66E-02	7.66E-07
XR kβ1	36.378	0.00672	4.36E-05	0.0023	5.10E-02	1.47E-06
XR Kβ2	37.255	0.00213	4.18E-05	0.0024	1.55E-02	4.45E-07
γ1	283.5	0.0000058	4.25E-05	0.004	4.29E-05	1.23E-09
γ2	661.657	0.851	9.91E-05	0.0039	1.47E+01	4.22E-04
β	Dist.	1	2.85E-07	0.0093	4.96E-02	1.43E-06
			.		**Total**	4.42E-04

Appendix H (Continued)

Table H.2: Simulated results from the Co-60 MCNP model.

RadioNuclide	**Activity [Bq]**		Measured Value [R/hr]			
Co-60	1.15E+05		1.06E-03			
Emission Type	**Energy [keV]**	**Intensity**	**MCNP [MeV/SP]**	**Error**	**MeV/s**	**[R/hr]**
γ1	347.14	0.000075	5.28E-05	0.0042	4.56E-04	1.31E-08
γ2	826.1	0.000076	1.21E-04	0.0037	1.05E-03	3.04E-08
γ3	1173.228	0.9985	1.62E-04	0.0033	1.86E+01	5.36E-04
γ4	1332.492	0.999826	1.80E-04	0.0032	2.07E+01	5.96E-04
γ5	2158.57	0.000012	2.68E-04	0.0034	3.70E-04	1.06E-08
γ6	2505.692	0.00000002	2.96E-04	0.0034	6.80E-07	1.96E-11
β	Dist	1	9.27E-08	0.0161	1.07E-02	3.07E-07
					Total	9.75E-04
CE k	1164.895	1.50E-04	3.35E-06	0.0095	5.77E-05	1.66E-09
CE L	1172.22	1.46E-05	3.36E-06	0.0094	5.66E-06	1.63E-10
CE N	1173.228	8.87E-08	3.35E-06	0.0094	3.41E-08	9.83E-13
CE M	1173.228	2.06E-06	3.35E-06	0.0094	7.93E-07	2.28E-11
CE K	1324.159	1.14E-04	4.48E-06	0.0105	5.86E-05	1.69E-09
CE L	1331.484	1.11E-05	4.79E-06	0.011	6.10E-06	1.76E-10
CE M	1332.492	1.56E-06	4.79E-06	0.0109	8.60E-07	2.48E-11
CE N	1332.492	6.73E-08	4.79E-06	0.0109	3.71E-08	1.07E-12
CE K	2150.24	5.30E-10	4.32E-03	0.0011	2.63E-07	7.58E-12
CE L	2157.56	5.20E-11	4.38E-03	0.0011	2.62E-08	7.55E-13
CE M	2158.57	7.30E-12	4.39E-03	0.0011	3.69E-09	1.06E-13
CE N	2158.57	3.20E-13	4.39E-03	0.0011	1.62E-10	4.65E-15
CE K	2497.359	1.60E-12	7.37E-03	0.0009	1.36E-09	3.91E-14
CE L	2504.684	1.50E-13	7.42E-03	0.0009	1.28E-10	3.69E-15
CE M	2505.692	2.10E-14	7.44E-03	0.0009	1.80E-11	5.17E-16
CE N	2505.692	9.20E-16	7.44E-03	0.0009	7.87E-13	2.27E-17
					Total	1.13E-03

Appendix H (Continued)

Table H.3: Simulated results from the Ba-133 MCNP model.

RadioNuclide	**Activity [Bq]**		Measured Value [R/hr]			
Ba-133	1.50E+05		2.78E-04			
Emission Type	**Energy [keV]**	**Intensity**	**MCNP [MeV/SP]**	**Error**	**MeV/s**	**[R/hr]**
XR kα2	30.625	0.339	6.03E-05	0.0019	3.06E+00	8.83E-05
XR kα1	30.973	0.622	5.89E-05	0.0019	5.49E+00	1.58E-04
XR kβ3	34.92	0.0588	4.72E-05	0.0022	4.17E-01	1.20E-05
XR kβ1	34.987	0.114	4.71E-05	0.0022	8.05E-01	2.32E-05
XR kβ2	35.818	0.0351	4.52E-05	0.0023	2.38E-01	6.85E-06
γ1	53.1622	0.0214	2.25E-05	0.0036	7.22E-02	2.08E-06
γ2	79.6142	0.0265	1.53E-05	0.0043	6.08E-02	1.75E-06
γ3	80.9979	0.329	1.52E-05	0.0043	7.48E-01	2.15E-05
γ4	160.612	0.00638	2.25E-05	0.0037	2.15E-02	6.20E-07
γ5	223.2368	0.00453	3.24E-05	0.0038	2.20E-02	6.33E-07
γ6	276.3989	0.0719	4.13E-05	0.004	4.45E-01	1.28E-05
γ7	302.8508	0.1834	4.57E-05	0.004	1.26E+00	3.62E-05
γ8	356.0129	0.6205	5.45E-05	0.0042	5.07E+00	1.46E-04
γ9	383.8485	0.0894	5.89E-05	0.0042	7.89E-01	2.27E-05
					total	5.33E-04

Table H.4: Simulated results from the Mn-54 MCNP model.

RadioNuclide	**Activity [Bq]**		**Measured Value [R/hr]**			
Mn-54	9.39E+03		3.10E-05			
Emission Type	**Energy [keV]**	**Intensity**	**MCNP [MeV/SP]**	**Error**	**MeV/s**	**[R/hr]**
Annihilation	511	6.00E-09	7.82E-05	0.0042	4.40E-09	1.27E-13
γ1	834.848	0.99976	1.22E-04	0.0036	1.14E+00	3.28E-05
					Total	3.28E-05

Appendix H (Continued)

Table H.5 Simulated results from the Am-241 MCNP model.

RadioNuclide	Activity [Bq]		Measured Value [R/hr]			
Am-241	3.59E+04		1.50E-05			
Emission Type	**Energy**	**Intensity**	**MCNP [MeV/SP]**	**Error**	**MeV/s**	**[R/hr]**
γ1	26.3446	0.0227	7.92E-05	0.0016	6.45E-02	1.86E-06
γ2	33.196	0.00126	5.20E-05	0.0021	2.35E-03	6.77E-08
γ3	42.704	0.000055	3.25E-05	0.0028	6.41E-05	1.85E-09
γ4	43.42	0.00073	3.15E-05	0.0029	8.26E-04	2.38E-08
γ5	55.56	0.000181	2.11E-05	0.0037	1.37E-04	3.96E-09
γ6	59.5409	0.359	1.93E-05	0.0039	2.48E-01	7.15E-06
γ7	64.83	0.00000145	1.75E-05	0.0041	9.09E-07	2.62E-11
γ8	67.45	0.0000042	1.68E-05	0.0042	2.54E-06	7.31E-11
γ9	69.76	0.000029	1.63E-05	0.0042	1.70E-05	4.90E-10
γ10	75.8	0.0000059	5.47E-06	0.0043	1.16E-06	3.33E-11
XR kα2	97.069	0.0000114	1.52E-05	0.0041	6.22E-06	1.79E-10
γ11	98.97	0.000203	1.53E-05	0.0041	1.11E-04	3.20E-09
XR kα1	101.059	0.0000181	1.53E-05	0.0041	9.95E-06	2.87E-10
γ12	102.98	0.000195	1.55E-05	0.0041	1.09E-04	3.13E-09
XR kβ3	113.303	0.00000227	1.63E-05	0.0039	1.33E-06	3.83E-11
XR kβ1	114.234	0.0000243	1.64E-05	0.0039	1.43E-05	4.13E-10
XR kβ2	117.463	0.00000168	1.67E-05	0.0039	1.01E-06	2.91E-11
γ13	123.052	0.00001	1.74E-05	0.0039	6.24E-06	1.80E-10
γ14	125.3	0.0000408	1.76E-05	0.0038	2.58E-05	7.44E-10
γ15	146.55	0.00000461	2.03E-05	0.0037	3.36E-06	9.68E-11
γ16	169.56	0.00000173	2.39E-05	0.0037	1.48E-06	4.27E-11
γ17	208.01	0.00000791	3.00E-05	0.0038	8.52E-06	2.46E-10
γ18	322.52	0.00000152	4.90E-05	0.0041	2.67E-06	7.70E-11
γ19	332.35	0.00000149	5.05E-05	0.0041	2.70E-06	7.77E-11
γ20	335.37	0.00000496	5.10E-05	0.0041	9.07E-06	2.61E-10
γ21	368.65	0.00000217	5.63E-05	0.0042	4.39E-06	1.26E-10
γ22	376.65	0.00000138	5.78E-05	0.0042	2.86E-06	8.25E-11
γ23	662.4	0.00000364	9.94E-05	0.0039	1.30E-05	3.74E-10
γ24	722.01	0.00000196	1.07E-04	0.0038	7.52E-06	2.17E-10
					Total	9.12E-06

Appendix I: Fluke Biomedical 451P – RYR Pressurized Ionization Chamber Muon and Anti-Muon Stopping Power Calculation

Stopping Power Calulcation								
Fluke Biomedical-451P RYR PIC			**Muon**			**Anti-Muon**		
Mean Momentum [MeV/c]	**β^2**	**F(B)**	**dE/dX [MeV/cm]**	**Intensity**	**Weighted Average [Mev/cm]**	**dE/dX [MeV/cm]**	**Intensity**	**Weighted Average [Mev/cm]**
250	9.12E-01	1.62E+01	1.98E-02	6.72E-02	1.33E-03	1.98E-02	6.84E-02	1.35E-03
350.00	9.46E-01	1.67E+01	1.99E-02	9.55E-02	1.90E-03	1.99E-02	9.69E-02	1.93E-03
470	9.66E-01	1.72E+01	2.03E-02	1.12E-01	2.28E-03	2.03E-02	1.16E-01	2.35E-03
620	9.79E-01	1.77E+01	2.08E-02	1.17E-01	2.43E-03	2.08E-02	1.21E-01	2.51E-03
780	9.86E-01	1.81E+01	2.13E-02	1.11E-01	2.35E-03	2.13E-02	1.16E-01	2.47E-03
920	9.89E-01	1.84E+01	2.17E-02	1.03E-01	2.23E-03	2.17E-02	1.09E-01	2.37E-03
1100	9.92E-01	1.87E+01	2.21E-02	9.30E-02	2.06E-03	2.21E-02	1.01E-01	2.23E-03
1300	9.94E-01	1.90E+01	2.25E-02	8.04E-02	1.81E-03	2.25E-02	8.84E-02	1.99E-03
1500	9.96E-01	1.93E+01	2.29E-02	7.16E-02	1.64E-03	2.29E-02	7.92E-02	1.82E-03
1840	9.97E-01	1.97E+01	2.35E-02	5.78E-02	1.36E-03	2.35E-02	0.00E+00	0.00E+00
2490	9.98E-01	2.02E+01	2.44E-02	3.58E-02	8.73E-04	2.44E-02	3.99E-02	9.72E-04
3490	9.99E-01	2.09E+01	2.54E-02	2.43E-02	6.15E-04	2.54E-02	2.74E-02	6.94E-04
4780	1.00E+00	2.15E+01	2.63E-02	1.45E-02	3.82E-04	2.63E-02	1.68E-02	4.41E-04
6210	1.00E+00	2.20E+01	2.71E-02	8.61E-03	2.33E-04	2.71E-02	1.01E-02	2.75E-04
8370	1.00E+00	2.26E+01	2.80E-02	4.90E-03	1.37E-04	2.80E-02	5.81E-03	1.63E-04
12420	1.00E+00	2.34E+01	2.92E-02	2.01E-03	5.87E-05	2.92E-02	2.36E-03	6.89E-05
18850	1.00E+00	2.42E+01	3.05E-02	7.29E-04	2.22E-05	3.05E-02	8.78E-04	2.68E-05
26680	1.00E+00	2.49E+01	3.16E-02	2.83E-04	8.93E-06	3.16E-02	3.65E-04	1.15E-05
36690	1.00E+00	2.55E+01	3.26E-02	1.28E-04	4.15E-06	3.26E-02	1.60E-04	5.20E-06
51470	1.00E+00	2.62E+01	3.36E-02	4.84E-05	1.63E-06	3.36E-02	5.81E-05	1.95E-06
72080	1.00E+00	2.69E+01	3.46E-02	2.01E-05	6.97E-07	3.46E-02	2.39E-05	8.29E-07
100960	1.00E+00	2.76E+01	3.57E-02	6.91E-06	2.47E-07	3.57E-02	8.55E-06	3.05E-07
				Total	2.17E-02		**Total**	2.17E-02

*** Both Muon and Anti-Muon weighted averages were normalized based on the muon + anti-muon (total) distribution and were summed together to obtain a total weighted stopping power,** $-\frac{dE}{dx} = 0.0217\,\frac{MeV}{cm}$

Appendix J: ADM-300 Multi-Functional Survey Meter Photon MCNP Results

Table J.1: Simulated results from the Cs-137 MCNP model.

Radionuclide	**Activity [Bq]**			**Measured Value [R/hr]:**	3.45E-04		
Cs-137	1.72E+05	**High range f4 tally**		**Low range f14 tally**			
Emission Type	**Energy [keV]**	**MCNP [#/cm^2*s]**	**Error**	**MCNP [#/cm^2*s]**	**Error**	**Total [#/ cm^{2}s]**	**[R/hr]**
γ1	283.5	3.25E-03	0.0086	1.51E-03	0.0033	4.76E-03	1.91E-09
γ2	661.657	5.74E+02	0.0077	2.83E+02	0.00029	8.57E+02	3.44E-04
					Total:	8.57E+02	3.45E-04

Table J.2: Simulated results from the Co-60 MCNP model.

Radionuclide	**Activity [Bq]**			**Measured Value [R/hr]:**	1.28E-03		
Co-60	1.09E+05	**High range f4 tally**		**Low range f14 tally**			
Emission Type	**Energy [keV]**	**MCNP [#/cm^2*s]**	**Error**	**MCNP [#/cm^2*s]**	**Error**	**Total [#/ cm^{2}s]**	**[R/hr]**
γ1	347.14	3.10E-02	0.0082	1.47E-02	0.0031	4.57E-02	1.84E-08
γ2	826.1	3.27E-02	0.0077	1.63E-02	0.0028	4.90E-02	1.97E-08
γ3	1173.228	4.35E+02	0.0076	2.19E+02	0.0028	6.53E+02	2.63E-04
γ4	1332.492	4.37E+02	0.0076	2.20E+02	0.0028	6.57E+02	2.64E-04
γ5	2158.57	5.36E-03	0.0075	2.50E-03	0.0028	7.86E-03	3.16E-09
γ6	2505.692	9.00E-06	0.0075	4.54E-06	0.0028	1.35E-05	5.44E-12
					Total:	9.47E-02	5.27E-04

Appendix J (Continued)

Table J.3: Simulated results from the Ba-133 MCNP model.

Radionuclide	**Activity [Bq]**			**Measured Value [R/hr]:**	1.48E-04		
Ba-133	1.46E+05	**High range f4 tally**		**Low range f14 tally**			
Emission Type	**Energy [keV]**	**MCNP [#/cm^2*s]**	**error**	**MCNP [#/cm^2*s]**	**error**	**Total [#/ cm^2s]**	**[R/hr]**
γ1	80.9979	4.21E+01	0.0168	2.06E+01	0.006	6.28E+01	2.52E-05
γ2	160.612	1.57E+00	0.0124	8.63E-01	0.0042	2.43E+00	9.79E-07
γ3	223.2368	1.8032	0.0095	8.49E-01	0.0036	2.65E+00	1.07E-06
γ4	276.3989	3.34E+01	0.0087	1.56E+01	0.0033	4.90E+01	1.97E-05
γ5	302.8508	8.95E+01	0.0084	4.20E+01	0.0032	1.31E+02	5.29E-05
γ6	356.0129	3.21E+02	0.0082	1.53E+02	0.0031	4.74E+02	1.91E-04
γ7	383.8485	4.71E+01	0.008	2.26E+01	0.003	6.97E+01	2.80198E-05
					Total:	7.92E+02	3.18E-04

Table J.4: Simulated results from the Mn-54 MCNP model.

Radionuclide	**Activity [Bq]**			**Measured Value [R/hr]:**	2.90E-05		
Mn-54	6.77E+03	**High range f4 tally**		**Low range f14 tally**			
Emission Type	**Energy [keV]**	**MCNP [#/cm^2*s]**	**error**	**MCNP [#/cm^2*s]**	**Error**	**Total [#/ cm^2s]**	**[R/hr]**
γ1	834.848	2.67E+01	0.0077	1.33E+01	0.0028	4.00E+01	1.61E-05

Appendix K: ADM-300 High Range Tube Muon and Anti-Muon Stopping Power Calculations

High Range GM tube			Muon			Anti-Muon		
Mean Momentum [MeV/c]	B^2	F(B)	dE/dX [MeV/cm]	Intensity	Weighted Average [MeV/cm]	dE/dX [MeV/cm]	Intensity	Weighted Average [Mev/cm]
250	9.117E-01	1.526E+01	2.041E-03	6.724E-02	1.372E-04	2.041E-03	6.841E-02	1.396E-04
350	9.462E-01	1.576E+01	2.065E-03	9.552E-02	1.972E-04	2.065E-03	9.691E-02	2.001E-04
470	9.663E-01	1.622E+01	2.113E-03	1.125E-01	2.376E-04	2.113E-03	1.157E-01	2.445E-04
620	9.788E-01	1.669E+01	2.175E-03	1.169E-01	2.542E-04	2.175E-03	1.209E-01	2.628E-04
780	9.858E-01	1.709E+01	2.235E-03	1.106E-01	2.472E-04	2.235E-03	1.163E-01	2.599E-04
920	9.894E-01	1.738E+01	2.282E-03	1.031E-01	2.352E-04	2.282E-03	1.095E-01	2.498E-04
1100	9.923E-01	1.770E+01	2.337E-03	9.300E-02	2.173E-04	2.337E-03	1.009E-01	2.358E-04
1300	9.943E-01	1.801E+01	2.390E-03	8.044E-02	1.922E-04	2.390E-03	8.836E-02	2.112E-04
1500	9.957E-01	1.828E+01	2.437E-03	7.164E-02	1.746E-04	2.437E-03	7.924E-02	1.931E-04
1840	9.970E-01	1.866E+01	2.506E-03	5.781E-02	1.449E-04	2.506E-03	0.000E+00	0.000E+00
2490	9.983E-01	1.924E+01	2.611E-03	3.582E-02	9.351E-05	2.611E-03	3.991E-02	1.042E-04
3490	9.991E-01	1.989E+01	2.731E-03	2.426E-02	6.624E-05	2.731E-03	2.736E-02	7.472E-05
4780	9.995E-01	2.050E+01	2.845E-03	1.452E-02	4.129E-05	2.845E-03	1.676E-02	4.768E-05
6210	9.997E-01	2.102E+01	2.940E-03	8.609E-03	2.531E-05	2.940E-03	1.015E-02	2.984E-05
8370	9.998E-01	2.160E+01	3.050E-03	4.902E-03	1.495E-05	3.050E-03	5.815E-03	1.774E-05
12420	9.999E-01	2.239E+01	3.197E-03	2.011E-03	6.428E-06	3.197E-03	2.360E-03	7.544E-06
18850	1.000E+00	2.321E+01	3.352E-03	7.289E-04	2.443E-06	3.352E-03	8.779E-04	2.943E-06
26680	1.000E+00	2.391E+01	3.481E-03	2.828E-04	9.845E-07	3.481E-03	3.648E-04	1.270E-06
36690	1.000E+00	2.454E+01	3.600E-03	1.276E-04	4.593E-07	3.600E-03	1.596E-04	5.747E-07
51470	1.000E+00	2.522E+01	3.727E-03	4.839E-05	1.803E-07	3.727E-03	5.815E-05	2.167E-07
72080	1.000E+00	2.589E+01	3.853E-03	2.011E-05	7.748E-08	3.853E-03	2.394E-05	9.225E-08
100960	1.000E+00	2.656E+01	3.979E-03	6.912E-06	2.751E-08	3.979E-03	8.551E-06	3.403E-08
					2.290E-03			2.284E-03

*** Both Muon and Anti-Muon weighted averages were normalized based on the muon + anti-muon (total) distribution and were summed together to obtain a total weighted stopping power,** $-\frac{dE}{dx} = 0.0022864\,\frac{MeV}{cm}$

Appendix L: ADM-300 Low Range Tube Muon and Anti-Muon Stopping Power Calculations

Low Range GM Tube			Muon			Anti-Muon		
Mean Momentum [MeV/c]	**B^2**	**F(B)**	**dE/dX**	**Intensity**	**Weighted Average [MeV/cm]**	**dE/dX [MeV/cm]**	**Intensity**	**Weighted Average [Mev/cm]**
2.500E+02	9.117E-01	1.526E+01	5.583E-04	6.724E-02	3.754E-05	5.583E-04	6.841E-02	3.820E-05
3.500E+02	9.462E-01	1.576E+01	5.650E-04	9.552E-02	5.397E-05	5.650E-04	9.691E-02	5.475E-05
4.700E+02	9.663E-01	1.622E+01	5.781E-04	1.125E-01	6.503E-05	5.781E-04	1.157E-01	6.690E-05
6.200E+02	9.788E-01	1.669E+01	5.950E-04	1.169E-01	6.955E-05	5.950E-04	1.209E-01	7.191E-05
7.800E+02	9.858E-01	1.709E+01	6.116E-04	1.106E-01	6.764E-05	6.116E-04	1.163E-01	7.112E-05
9.200E+02	9.894E-01	1.738E+01	6.246E-04	1.031E-01	6.437E-05	6.246E-04	1.095E-01	6.836E-05
1.100E+03	9.923E-01	1.770E+01	6.394E-04	9.300E-02	5.947E-05	6.394E-04	1.009E-01	6.452E-05
1.300E+03	9.943E-01	1.801E+01	6.540E-04	8.044E-02	5.260E-05	6.540E-04	8.836E-02	5.778E-05
1.500E+03	9.957E-01	1.828E+01	6.668E-04	7.164E-02	4.777E-05	6.668E-04	7.924E-02	5.284E-05
1.840E+03	9.970E-01	1.866E+01	6.856E-04	5.781E-02	3.964E-05	6.856E-04	0.000E+00	0.000E+00
2.490E+03	9.983E-01	1.924E+01	7.144E-04	3.582E-02	2.559E-05	7.144E-04	3.991E-02	2.851E-05
3.490E+03	9.991E-01	1.989E+01	7.473E-04	2.426E-02	1.813E-05	7.473E-04	2.736E-02	2.045E-05
4.780E+03	9.995E-01	2.050E+01	7.785E-04	1.452E-02	1.130E-05	7.785E-04	1.676E-02	1.305E-05
6.210E+03	9.997E-01	2.102E+01	8.047E-04	8.609E-03	6.927E-06	8.047E-04	1.015E-02	8.165E-06
8.370E+03	9.998E-01	2.160E+01	8.348E-04	4.902E-03	4.092E-06	8.348E-04	5.815E-03	4.854E-06
1.242E+04	9.999E-01	2.239E+01	8.748E-04	2.011E-03	1.759E-06	8.748E-04	2.360E-03	2.065E-06
1.885E+04	1.000E+00	2.321E+01	9.173E-04	7.289E-04	6.686E-07	9.173E-04	8.779E-04	8.053E-07
2.668E+04	1.000E+00	2.391E+01	9.527E-04	2.828E-04	2.694E-07	9.527E-04	3.648E-04	3.476E-07
3.669E+04	1.000E+00	2.454E+01	9.853E-04	1.276E-04	1.257E-07	9.853E-04	1.596E-04	1.573E-07
5.147E+04	1.000E+00	2.522E+01	1.020E-03	4.839E-05	4.935E-08	1.020E-03	5.815E-05	5.931E-08
7.208E+04	1.000E+00	2.589E+01	1.054E-03	2.011E-05	2.120E-08	1.054E-03	2.394E-05	2.525E-08
1.010E+05	1.000E+00	2.656E+01	1.089E-03	6.912E-06	7.527E-09	1.089E-03	8.551E-06	9.312E-09
					6.265E-04			6.249E-04

*** Both Muon and Anti-Muon weighted averages were normalized based on the muon + anti-muon (total) distribution and were summed together to obtain a total weighted stopping power,** $-\frac{dE}{dx} = 0.000625651\,\frac{MeV}{cm}$

Appendix M: Fluke Biomedical Copyright Permission

FLUKE.

June 8, 2017

Matt Gift
Graduate Student, Radiological Health Sciences Department
College of Veterinary Medicine and Biomedical Science,
Colorado State University, Fort Collins, CO, USA
mgift@colostate.edu

Re: Permission to Reproduce Copyrighted Material

Dear Matt,

Fluke Corporation is pleased to hereby grant permission to reproduce technical data sheet figures of the Fluke 451P Pressurized microR ion Chamber Survey Meter.

Permission is granted on the condition that you legibly reproduce the legend "Reproduced with Permission, Fluke Corporation".

It is our understanding from your request dated June 7, that the purpose for copying these figures is to include them in a research paper, and that the data sheet will not be copied for any other purpose.

Thank you for your cooperation, and for your interest in Fluke.

Sincerely,

Jeffrey Black

Fluke Corporation	Telephone	Facsimile	Internet
PO Box 9090 Everett WA 98206.9090 USA	425.347.6100	425.446.5116	www.fluke.com

<u>Appendix N: Mirion Technologies Copyright Permission</u>

Hi Matt,

Legal is asking if you have a copyright release agreement you would like us to sign. **If not, we have no objections to the inclusion of the curves in your paper.**

They did note that if you want to identify us by name, please use the following trademark attribution:

Mirion ® is a trademark of Mirion Technologies and/or its affiliates in the United States and other countries

Regards,

Steven

***Email communication on 6/15/2017 with Steven Bunch at Mirion Technologies**